

High-temperature electromechanical loss in piezoelectric langasite and catangasite crystals

Cite as: J. Appl. Phys. **130**, 085102 (2021); <https://doi.org/10.1063/5.0058751>

Submitted: 02 June 2021 • Accepted: 04 August 2021 • Published Online: 23 August 2021

 Yuriy Suhak, Holger Fritze, Andrei Sotnikov, et al.



View Online



Export Citation



CrossMark

ARTICLES YOU MAY BE INTERESTED IN

Plasma processing for advanced microelectronics beyond CMOS

Journal of Applied Physics **130**, 080901 (2021); <https://doi.org/10.1063/5.0053666>

Realization of highly rectifying Schottky barrier diodes and pn heterojunctions on κ -Ga₂O₃ by overcoming the conductivity anisotropy

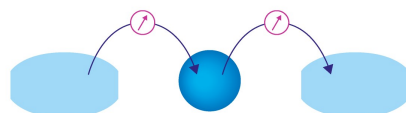
Journal of Applied Physics **130**, 084502 (2021); <https://doi.org/10.1063/5.0056630>

Frequency band-selected one-way topological edge mode via acoustic metamaterials and metasurface

Journal of Applied Physics **130**, 085101 (2021); <https://doi.org/10.1063/5.0058546>

Webinar

Interfaces: how they make or break a nanodevice



March 29th – Register now



Zurich
Instruments

High-temperature electromechanical loss in piezoelectric langasite and catangasite crystals

Cite as: J. Appl. Phys. **130**, 085102 (2021); doi: [10.1063/5.0058751](https://doi.org/10.1063/5.0058751)

Submitted: 2 June 2021 · Accepted: 4 August 2021 ·

Published Online: 23 August 2021



View Online



Export Citation



CrossMark

Yuriy Suhak,^{1,a)}  Holger Fritze,¹ Andrei Sotnikov,² Hagen Schmidt,² and Ward L. Johnson³

AFFILIATIONS

¹Institute of Energy Research and Physical Technologies, Clausthal University of Technology, Am Stollen 19B, Goslar 38640, Germany

²Leibniz Institute for Solid State and Materials Research Dresden, Helmholtzstr. 20, Dresden 01069, Germany

³National Institute of Standards and Technology, 325 Broadway St., Boulder, Colorado 80305, USA

^{a)}Author to whom correspondence should be addressed: yuriy.suhak@tu-clausthal.de

ABSTRACT

Temperature-dependent acoustic loss Q^{-1} is studied in partially disordered langasite (LGS, $\text{La}_3\text{Ga}_5\text{SiO}_{14}$) and ordered catangasite (CTGS, $\text{Ca}_3\text{TaGa}_3\text{Si}_2\text{O}_{14}$) crystals and compared with previously reported CTGS and langatate (LGT, $\text{La}_3\text{Ga}_{5.5}\text{Ta}_{0.5}\text{O}_{14}$) data. Two independent techniques, a contactless tone-burst excitation technique and contacting resonant piezoelectric spectroscopy, are used in this study. Contributions to the measured $Q^{-1}(T)$ are determined through fitting to physics-based functions, and the extracted fit parameters, including the activation energies of the processes, are discussed. It is shown that losses in LGS and CTGS are caused by a superposition of several mechanisms, including intrinsic phonon-phonon loss, point-defect relaxations, and conductivity-related relaxations.

© 2021 Author(s). All article content, except where otherwise noted, is licensed under a Creative Commons Attribution (CC BY) license (<http://creativecommons.org/licenses/by/4.0/>). <https://doi.org/10.1063/5.0058751>

I. INTRODUCTION

Piezoelectric resonant sensors that can be operated at high temperatures and in harsh environments are needed in the aerospace, automotive, and energy industries. Anticipated applications of such sensors include structural health monitoring and measurements of mass adsorption or deposition, temperature, pressure, and gas constituents.^{1–3} The sensing principles of piezoelectric resonators are based on frequency shifts that arise from variations in externally determined factors, such as temperature, mass load^{4,5} or viscoelastic effects of films^{6,7} or, in general, of the surrounding medium.⁸ It is advantageous to operate these sensors in a thickness-shear mode (TSM), since such modes do not lose vibrational energy through the generation of compressive waves in a surrounding medium. To provide enhanced specificity and sensitivity in chemical sensing, films that selectively bond to specific molecules can be deposited onto a resonator surface. This can enable, for example, the sensing of specified gas constituents in the ppm range.^{9,10}

However, the application of piezoelectric materials at high temperatures faces many challenges and limitations. Polycrystalline ceramics like PZT [$\text{Pb}(\text{Zr}_{1-x}\text{Ti}_x)\text{O}_3$] cannot be used above $\sim 300^\circ\text{C}$ due to their low Curie temperature, high electrical conductivity, and strong damping associated with grain boundaries.^{11,12}

Quartz (SiO_2) undergoes a structural phase transformation from α - to β -quartz at 573°C .^{13,14} It belongs to the point group 32 in the α -phase and to the point group 622 in the β -phase. Quartz is reported to show piezoelectric response above the α - to β -phase transformation temperature;¹⁴ however, due to the higher crystal symmetry, Y-cut resonators operated in TSM cannot be used in the β -phase, and rotated cuts must be used, instead.¹⁴ Ferroelectrics, such as congruent lithium niobate (LiNbO_3) and lithium tantalate (LiTaO_3), either decompose above $\sim 300^\circ\text{C}$,^{13,15} which prevents their long-term application, or exhibit a ferroelectric-paraelectric phase transformation at $\sim 630^\circ\text{C}$, respectively.¹⁶ Stoichiometric LiNbO_3 has been excited piezoelectrically up to at least 900°C ;¹⁷ however, a strong decrease in the resonator quality factor Q occurs above 600°C , which is associated with lithium loss and, therefore, irreversible material degradation.

Aluminum nitride (AlN) is reported to be characterized at temperatures above 1000°C .¹⁸ However, its poor oxidation resistance above 700°C limits its use in air or oxidizing atmospheres.^{18,19} In addition, mass production of AlN bulk crystals remains challenging, due to the extremely high melting temperature ($\sim 2200^\circ\text{C}$) and difficulties in obtaining sufficiently large bulk crystal boules with high structural perfection.²⁰

Gallium orthophosphate (GaPO_4) is an excellent material that possesses a relatively high electromechanical coupling and low dielectric loss with a crystallographic phase transformation at about 970°C . This material has been successfully operated at temperatures up to at least 900°C .²¹ However, similarly to AlN, the availability of GaPO_4 is limited because of the difficult and expensive growth process.²² Other examples of promising piezoelectric materials for high-temperature applications are calcium oxyborate single crystals ($\text{ReCa}_4\text{O}(\text{BO}_3)_3$, where “Re” denotes a rare earth element). These materials show no phase transformation up to their melting point at about 1500°C and possess exceptionally low electrical conductivity and stable piezoelectric properties. They are, however, pyroelectric, which could be problematic when induced charge has to be measured.²³ The reported range of operating temperatures for $\text{ReCa}_4\text{O}(\text{BO}_3)_3$ extends to at least 1000°C .²⁴

Piezoelectric crystals from the so-called “langasite family” have attracted much attention over the past three decades. These compounds possess piezoelectric coefficients that are two to three times greater than those of quartz, have no phase transition up to their melting points (1300 – 1500°C), are non-pyroelectric, and can be grown in the form of large high-quality crystals by the Czochralski technique.^{25–27} These crystals belong to the trigonal space group $P321$ (point group 32) with the general formula $\text{A}_3\text{BC}_3\text{D}_2\text{O}_{14}$ and are generally classified into two types, partially disordered and ordered, depending on the ionic distribution. In partially disordered crystals, the same element can enter different cationic sites, while in ordered crystals, each cationic site is occupied by a specific element.^{28,29} Generally, ordered crystals show improved electromechanical properties, including lower electrical conductivity.^{30,31} Two structurally disordered compounds, langasite ($\text{La}_3\text{Ga}_5\text{SiO}_{14}$, LGS) and langatate ($\text{La}_3\text{Ga}_{5.5}\text{Ta}_{0.5}\text{O}_{14}$, LGT), as well as structurally ordered catangasite ($\text{Ca}_3\text{TaGa}_3\text{Si}_2\text{O}_{14}$, CTGS) are subjects of this study.

The use of bulk acoustic wave (BAW) resonators as high-temperature sensors^{1,2,32} requires maximization of the acoustic quality factor Q , since a lower Q results in uncertainty in resonant frequency determination and, therefore, limits the resolution in sensing applications. Previously reported investigations of loss, Q^{-1} , in LGS and LGT revealed that the dominant contribution to the loss switches between several physical mechanisms as a function of temperature.^{33–38} However, the nature of these mechanisms remains a subject of research. In Refs. 34 and 37, temperature-dependent loss peaks in LGS between room temperature and 500°C are attributed to anelastic point defect relaxations superimposed on a loss contribution with a very broad temperature dependence. The latter is hypothesized as arising from a dislocation kink migration mechanism. Similarly to LGS, two peaks in an LGT crystal between 20 and 500°C are attributed to point defect relaxations.³⁷ No evidence for a broadly temperature-dependent loss contribution was found in this LGT crystal, and, since the crystal had a relatively low dislocation density, the data on this sample support the hypothesis of a dislocation source for the broadly temperature-dependent background in LGS.³⁷ Fritze *et al.*^{35,36} provided evidence that the high-temperature loss in LGS (i.e., above 600°C) is dominated in the low megahertz range by piezoelectric/carrier relaxation. Hirschle and Schreuer³⁸ attributed the high-temperature loss at frequencies below 700 kHz in LGS and LGT to either a

combination of two different point defect relaxations or a combination of piezoelectric/carrier and point-defect relaxation and noted that the relative magnitude of these potential contributions could not be determined in the absence of information extending beyond their data, which exclusively included acoustic loss.

Fewer high-temperature studies of $Q^{-1}(T)$ in CTGS crystals have been published. In our previous reports,^{39–41} loss peaks below 700°C were attributed to point defect relaxations, and in Ref. 42, losses above 700°C were attributed primarily to the piezoelectric/carrier relaxation.

In this article, $Q^{-1}(T)$, electrical conductivity, and dielectric constants of structurally ordered CTGS and partially disordered LGS are presented. The data for $Q^{-1}(T)$ are fit to functions with terms representing several physical mechanisms.³⁷ A combined analysis of the loss and conductivity data leads to a clear identification of piezoelectric/carrier loss as the dominant contribution to Q^{-1} in the studied specimens in the highest measured temperature range (above approximately 700°C in CTGS and 800°C in LGS). In addition, the analysis provides a new understanding of the loss in LGS involving a superposition of two piezoelectric/carrier relaxations associated with electronic and ionic conduction. At intermediate temperatures, point-defect relaxations substantially contribute to the loss in all of the specimens. Similarities in some of the activation energies of these relaxations indicate the presence of point defects with similar symmetry in CTGS and LGS, as well as previously studied langatate LGT.

II. SPECIMENS

Nominally undoped LGS and CTGS resonators used in this study were prepared as Y-cut plano-plano disks from crystals grown by the Czochralski technique. One LGS resonator, designated LGS-01, with a fundamental frequency near 850 kHz and 10 mm diameter was manufactured from a crystal grown by FOMOS-Materials (Moscow, Russia) (The identification of commercial products is provided for technical completeness and does not reflect an endorsement by NIST.). Another LGS resonator with a fundamental frequency near 5.4 MHz and 10 mm diameter was received from the Leibniz-Institute for Crystal Growth (Berlin, Germany). This resonator is designated LGS-02.

CTGS resonators were fabricated by FOMOS-Materials (Moscow, Russia). One CTGS plate, designated CTGS-01, has a thickness of 0.3 mm and was used for electrical conductivity measurements. Another resonator, designated CTGS-02, has a TSM fundamental frequency near 6 MHz and was used for the study of acoustic losses. The third CTGS resonator, designated CTGS-03, with a diameter of 10 mm and fundamental frequency near 5 MHz , was used for both electrical and acoustic studies.

One Y-cut LGT resonator, designated LGT, was manufactured at the Advanced Materials Processing and Analysis Center of the University of Central Florida and is used in this study to provide a comparison of temperature-dependent losses with those of CTGS and LGS. This resonator is a plano-convex disk with a diameter of 14 mm and fundamental frequency of 2 MHz . The spherical surface has a radius of 265 mm (2 diopter). The CTGS-01, CTGS-02, and LGS-02 specimens are colorless, while LGS-01 and CTGS-03 have a light orange tint.

TABLE I. Sample labels, dimensions, fundamental frequencies, and study methods.

Sample label	Cut	Diameter of		Frequency or thickness	Study
		resonator (nm)	electrode (nm)		
LGS-01	Y	10	5	850 kHz	Conductivity/loss
LGS-02	Y	10	5	5.43 MHz	Conductivity/loss
LGS-03	Y	10	5	0.3 mm	Dielectric constant
CTGS-01	Y	14	6	0.3 mm	Conductivity
CTGS-02	Y	14	n/a	6 MHz	Loss
CTGS-03	Y	10	5	5 MHz	Conductivity/loss
CTGS-04	Y	n/a ^a	n/a ^a	0.5 mm	Dielectric constant
LGT	Y	14	n/a	2 MHz	Loss

^aCTGS-04 was a rectangular plate with dimensions of $8 \times 8 \times 0.5 \text{ mm}^3$. The dimensions of the electrodes were $8 \times 8 \text{ mm}^2$.

For conductivity measurements and resonant piezoelectric spectroscopy (RPS) performed at the Clausthal University of Technology (TUC), the specimens were coated with keyhole-shaped platinum electrodes. For the LGS-02 specimen, pulsed laser deposition (PLD)⁴³ was used, resulting in electrodes with $\sim 300 \text{ nm}$ thickness. For the LGS-01, CTGS-01, and CTGS-03 specimens, more high-temperature stable Pt electrodes with a thickness of $\sim 3 \mu\text{m}$ were deposited by screen printing (print ink: Ferro Corporation, No. 6412 0410). After screen printing, the resonators were annealed at 1000°C for $\sim 30 \text{ min}$. The specimen labels, orientations, dimensions, and fundamental frequencies are summarized in Table I along with the types of measurements that were employed.

Additionally, a rectangular CTGS plate, designated CTGS-04, with dimensions of $8 \times 8 \times 0.5 \text{ mm}^3$ was prepared for dielectric constant measurements from the crystal grown by Fomos-Materials. These measurements were performed at the Leibniz Institute for Solid State and Material Research (Dresden, Germany). The measurements of LGS dielectric constant were performed on an LGS plate with a diameter of 10 mm and a thickness of 0.3 mm . This sample, designated LGS-03, was manufactured from a crystal grown by the Leibniz Institute for Crystal Growth.

III. MEASUREMENT AND ANALYSIS TECHNIQUES

A. Electrical conductivity and dielectric constants

Investigation of bulk properties was performed by AC impedance spectroscopy in a frequency range of 1 Hz to 1 MHz using an impedance/gain-phase analyzer (Solartron 1260). An electrical equivalent-circuit model consisting of a constant phase element connected in parallel with a bulk resistance R_B was fitted to the measured data. The bulk conductivity σ was calculated from the relation $\sigma = t(A \times R_B)^{-1}$, where t and A are the thicknesses of the sample and electrode area, respectively. The lead

resistance, arising from cables/mounting, did not exceed 10Ω , which corresponds to approximately 0.02% of the resistance of CTGS at 1000°C . Therefore, it was ignored in the fitting procedure.

The dielectric constants ϵ_{11} for LGS and CTGS were determined using the same impedance/gain-phase analyzer at a frequency of 10 kHz , which was far below the mechanical resonance frequency of the samples.

B. Electromechanical losses

Electromechanical losses of the specimens were determined at the Clausthal University of Technology (TUC) and the National Institute of Standards and Technology (NIST) using two different experimental setups.

The measurements at the TUC were performed by means of RPS, which employed stepped-frequency direct piezoelectric excitation of Pt-electroded samples mounted on an aluminum oxide sample holder. In this system, platinum foils provide electrical contact to the electrodes on each side of the sample. With the aim of minimizing damping from mechanical contact, only small areas near the edges of the resonator are electrically contacted and mechanically clamped. The sample holder and resonator are placed in a tube furnace that enables heating up to 1500°C . The measurements are performed in air at atmospheric pressure while heating at a rate of 1 K/min from ambient temperature.

The resonance spectra of TSM resonators are acquired in the vicinity of the resonance frequency through the use of a high-speed network analyzer Agilent E5100A. The measured real and imaginary parts of the impedance are transformed into the admittance. Subsequently, a Lorentz function is fitted to the real part of the admittance (conductance, G) as a function of frequency f ,

$$G(f) = \frac{2A}{\pi} \frac{\Delta f_s'}{4(f-f_s)^2 + \Delta f_s'^2}, \quad (1)$$

where f_s is the series resonant frequency, $\Delta f_s'$ is the full width of the peak at half maximum (FWHM) of the Lorentzian, and A is a fitting parameter. The quality factor of the resonator is then calculated from the relation $Q = f_s/\Delta f_s$,⁴⁴ where Δf_s corresponds to the FWHM of the squared conductance G^2 and is approximated as $\Delta f_s \approx 0.64 \Delta f_s'^2$.

The described approach is valid for materials with low losses at the measurement temperature, where the conductance G of the resonator is negligible except at frequencies in the vicinity of the resonance frequency. With increasing temperature, the background G also increases, and, consequently, the frequency dependence of G is not accurately given by Eq. (1). Therefore, the method of analysis must be modified to evaluate losses at high temperatures. Following Ref. 2, the Q -factor is given by

$$Q = \frac{f_s}{\Delta f_s} \frac{G_{\text{max}} - G_s}{G_{\text{max}}}, \quad (2)$$

where G_{max} is the maximum of the conductance in the resonance and G_s is a static conductance.² Equation (2) was used to evaluate the Q -factor of all the specimens measured with the RPS technique.

Acoustic-resonance measurements at the NIST were performed on bare crystals (without electrodes) that were supported at three points near their edges by sapphire spheres, as described elsewhere.⁴⁰ Piezoelectric excitation and detection were accomplished with noncontacting copper electrodes spaced approximately 1 mm apart. The electrodes were driven by a gated sine wave (tone burst) and provided passive detection of vibrations during resonant ring-down after the tone burst through the inverse piezoelectric effect. The duration of the tone bursts was 3 ms, with the exception of 1 ms bursts in measurements of the fundamental mode of CTGS-02. A phase sensitive receiver was employed to extract the components of the signal that were in phase and out of phase with the reference gated sinusoid during ringdown. The logarithmic decrement at each measurement temperature was determined from an exponential fit of signal amplitude vs ringdown time and then translated to the corresponding Q^{-1} . The resonant frequency was determined in real time from a linear fit of the phase (relative to the reference) vs ringdown time.⁴⁵ After each frequency measurement during temperature ramps, the reference frequency was adjusted to approximately match the anticipated resonant frequency of the next measurement based on the current measured rate of change of resonant frequency with temperature. Measurements were obtained during cooling at a rate of (1.0 ± 0.2) K/min above approximately 280 °C in high vacuum ($< 3 \times 10^{-4}$ Pa) and at a lower rate below this temperature due to a lower passive thermal exchange. Helium was introduced below 100 °C to expedite cooling. Pressures below these temperatures were less than 150 Pa.

C. Analysis of loss contributions

Based on our previous studies of CTGS,^{39–42} as well as other studies of acoustic loss in LGS and LGT,^{33–38} the following dissipation mechanisms that can contribute to the overall loss in TSM resonator were initially considered:

- (1) intrinsic phonon–phonon interactions,
- (2) point defect relaxations,
- (3) piezoelectric/carrier relaxation (conductivity-related losses), and
- (4) non-material contribution (cables, mounting, etc.).

1. Phonon–phonon loss

Phonon–phonon scattering can be the dominant loss mechanism at near room temperature (and below) for high-quality piezoelectric crystals with efficient vibrational trapping or minimal mechanical contact to the crystal.^{46,47} Propagating or standing acoustic waves in a solid lead to a dynamic distortion in thermal-phonon energy levels, and the resultant redistribution of the system toward momentary local thermal equilibrium occurs through a relaxation of the phonon population from the perturbed state to the equilibrium state via phonon–phonon collisions. The entropy produced by this relaxation dissipates the energy of the sound wave. Depending on the relaxation time of the phonons, this scattering process can be divided into two regimes: the Landau–Rumer regime, for which the acoustic-wave period is shorter than the phonon relaxation time (τ_{ph}), and the Akhiezer regime, for which the wave period is longer than τ_{ph} .^{48,49} For resonators operated in

the megahertz range, as in this work, the Akhiezer regime is appropriate.^{46,47,50} This contribution to acoustic loss is approximately proportional to the resonant frequency and exhibits only weak temperature dependence above room temperature.⁴⁶ The maximum of Qf , limited by Akhiezer damping, has been found to be on the order of 10^{13} Hz for quartz, LGS, and LGT resonators.^{37,46,50}

2. Point defect relaxations

Anelastic relaxation can arise from point defects, which produce local anisotropic distortions in the crystal lattice. The application of acoustic stress leads to time-delayed thermally activated reorientation of these defects—anelastic defect relaxation. This process is dependent on frequency and temperature and is described, for each defect species, by a Debye function,

$$Q^{-1}(\omega, T) = \frac{\Delta}{T} \frac{\omega\tau}{1 + \omega^2\tau^2}, \quad (3)$$

where Δ is a temperature-independent constant proportional to the concentration of the defect species, T is the absolute temperature, ω is the angular acoustic frequency (equal to $2\pi f$), and τ is the reorientation relaxation time of the defect. Since the reorientation of defects occurs by thermally activated jumps over potential barriers, the relaxation time has an Arrhenius dependence on temperature,

$$\tau = \gamma \exp\left(\frac{E_A}{kT}\right), \quad (4)$$

where γ is a time constant, E_A is an activation energy, and k is the Boltzmann constant. The theory of anelastic relaxations in crystalline solids is summarized in Ref. 51.

3. Piezoelectric/carrier relaxation

At sufficiently elevated temperatures, the piezoelectric/carrier relaxation mechanism contributes significantly to the overall loss, becoming, in some cases, the dominant contribution.^{52,36} These conductivity-related losses are caused by the motion of charge carriers in an oscillating piezoelectric field. According to Hutson and White,⁵² this contribution can be described by the following equation:

$$Q_c^{-1}(\omega, T) = K^2 \frac{\omega_c/\omega}{1 + 2(\omega_c/\omega_D) + (\omega/\omega_D)^2 + (\omega_c/\omega)^2} = K^2 \frac{\omega/\omega_c}{1 + (\omega/\omega_c)^2 + 2\zeta + \zeta^2}, \quad (5)$$

with $\zeta = \omega^2/(\omega_c\omega_D)$. In this equation, K^2 is the electromechanical coupling coefficient, $\omega_c = 2\pi f_c$ is the dielectric relaxation frequency, and ω_D is the diffusion frequency.

The electromechanical coefficient K^2 is defined as the ratio of time-averaged stored elastic energy to time-averaged input electrical energy. In this study, only Y-cut resonators operated in the thickness-shear mode are investigated, and no other vibrational modes are considered. Consequently, for the thickness-shear mode of Y-cut trigonal crystals, K^2 is equal to $e_{11}^2/(C_{66}\epsilon_{11})$ in

reduced-index notation, where e_{11} is a piezoelectric coefficient, C_{66} is an elastic stiffness, and ϵ_{11} is a dielectric permittivity.

The dielectric relaxation frequency is given by

$$\omega_c = \frac{\sigma}{\epsilon_{11}}, \quad (6)$$

where σ is the electrical conductivity. The diffusion frequency is given by $\omega_D = (qC_{66})/(kTp\mu\rho)$,⁵² where q is the elementary charge, μ is the carrier mobility, ρ is the density, and p is the fraction of the acoustically produced space charge that is mobile.

The maximum of the parameter ζ was estimated for LGS in Ref. 37. At 14 MHz and 470 °C, it was found to be on the order of 10^{-9} , so that $\zeta \ll 1$. Therefore, in that case, terms involving ζ in Eq. (5) could be ignored. A similar estimate of the upper bound for ζ for CTGS can employ values determined here for ϵ_{11} (see Sec. IV A) as well as C_{66} and ρ and from our previous report,⁵³ but data on μ are not available for CTGS. In the absence of carrier mobility data, an estimate is performed using the values of μ obtained from donor-doped LGS⁵⁴ at temperatures where its conductivity is, as in CTGS, predominantly electronic (see Sec. IV A). Following the procedure in Ref. 37, this leads to an estimate of $0.002 \cdot p$ (with $p < 1$) for ζ at 900 °C and 5 MHz. Since donor-doped langasite shows approximately two orders of magnitude greater conductivity than CTGS at elevated temperatures, it is reasonable to assume that the carrier mobility in LGS is not lower than that in CTGS. Therefore, since ζ is proportional to μ , one can expect its value for CTGS at 900 °C and 5 MHz to be equal or smaller than the estimate of $0.002 \cdot p$, and the dependence of Q^{-1} on carrier diffusion can be ignored. Under this approximation, Eq. (5) assumes a simple Debye form,

$$Q_c^{-1}(\omega, T) \approx K^2 \frac{\omega/\omega_c}{1 + (\omega/\omega_c)^2} = K^2 \frac{\omega\tau_c}{1 + \omega^2\tau_c^2}, \quad (7)$$

where the dielectric relaxation time τ_c is equal to $1/\omega_c$. This piezoelectric/carrier relaxation contribution has a maximum at the temperature where the dielectric relaxation frequency ω_c is equal to the acoustic frequency.

The temperature dependence of ω_c is primarily determined by that of σ . As reported in Ref. 36, σ in LGS below 700 °C is governed by the electronic conduction mechanism and can be written as

$$\sigma = \sigma_0 \exp\left(-\frac{E_c}{kT}\right), \quad (8)$$

where E_c is an activation energy and σ_0 is a pre-exponential constant. Above 700 °C, the oxygen ion conduction mechanism becomes dominant and the conductivity is assumed to have the form

$$\sigma = \frac{\sigma_0}{T} \exp\left(-\frac{E_c}{kT}\right). \quad (9)$$

Therefore, according to theory developed in Ref. 52, two different conduction mechanisms are expected to contribute to the overall acoustic loss in LGS.

From Eqs. (6), (8), and (9), the dielectric relaxation time can be written for ionic and electronic conduction mechanisms as

$$\tau_{c(\text{electronic})} = \frac{\epsilon_{11}}{\sigma_0} \exp\left(\frac{E_c}{kT}\right) = \gamma_c \exp\left(\frac{E_c}{kT}\right), \quad (10)$$

$$\tau_{c(\text{ionic})} = \frac{\epsilon_{11}T}{\sigma_0} \exp\left(\frac{E_c}{kT}\right) = \gamma_c T \exp\left(\frac{E_c}{kT}\right). \quad (11)$$

In a previous report,⁴² it was shown that, even at the highest measured temperatures (~ 1300 °C), the contribution of oxygen ions to the overall conductivity of CTGS does not exceed 0.1%. This leads to the conclusion that electronic conduction is dominant, assuming that the contribution of protons and cations is small. The latter assumption is proven for LGS.³⁶ Therefore, the conductivity for CTGS is understood to have the form given by Eqs. (8).^{36,42}

4. Non-material contribution

Finally, a non-material-related contribution, which arises from acoustic energy loss to electrical lines and mounting, is assumed to be temperature and frequency independent and, therefore, described by a constant C_0 .

5. Total loss

Considering the above-described physical mechanisms, the following general expression was employed to fit the measured Q^{-1} of resonators in this study:

$$Q^{-1}(\omega, T) = \sum_{i=1}^n \frac{\Delta_i}{T} \frac{\omega\tau_i}{1 + \omega^2\tau_i^2} + \sum_{j=1}^2 K^2 \frac{\omega\tau_c}{1 + \omega^2\tau_c^2} + B\omega + C_0. \quad (12)$$

The first term in this equation represents the contributions of anelastic point defect relaxations from n defect species. The second term represents piezoelectric/carrier relaxation associated with electronic ($j=1$) and if applicable, ionic ($j=2$), conduction mechanisms. The term $B\omega$ approximates the intrinsic phonon-phonon loss. The term C_0 describes an approximately constant contribution that arises from acoustic energy loss that is not within the material. As described below, the specific number of point-defect relaxations (n) and number of piezoelectric/carrier relaxations included in the fits of Q^{-1} varied between samples, based on the number of observed peaks and, in the case of CTGS, evidence for an insignificant contribution from ionic conduction. The general approach seeks to optimize the robustness of fitting algorithms by including only a minimal number of terms that provide a close match to the data. Consistent with this approach, Eq. (12) does not include a broad temperature-dependent background of the types previously employed in some analyses of temperature-dependent loss of LGS and CTGS.^{37–39} The magnitudes of such temperature-dependent backgrounds have previously been found to be correlated with a difference in dislocation density,³⁷ and, therefore, it would not be surprising to find that they can be ignored, relative to other contributions, in the specific samples included in this study.

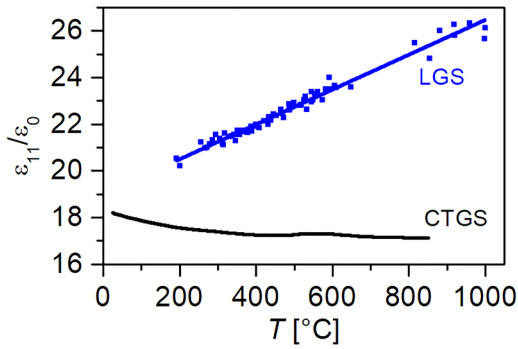


FIG. 1. Relative dielectric constants ϵ_{11}/ϵ_0 of LGS-03 and CTGS-04 as a function of temperature. The solid line for LGS specimen represents the linear fit of measured data.

IV. MEASUREMENTS AND ANALYSIS

A. Dielectric constants and electrical conductivity

The temperature dependences of the relative dielectric constants ϵ_{11}/ϵ_0 of both LGS and CTGS are shown in Fig. 1. Here, ϵ_0 denotes the dielectric constant of free space. As seen from Fig. 1, the ϵ_{11} of LGS increases approximately linearly with temperature, reaching a value of (26.1 ± 1.3) at the highest measured temperature (1000 °C), while the ϵ_{11} of CTGS decreases, overall, with increasing temperature. At 850 °C, the relative dielectric constant of CTGS is (17.1 ± 0.8) .

The electrical conductivities σ of LGS-01 and LGS-02 are shown in Fig. 2. For the sake of clarity, only every tenth data point is shown for LGS-01. As seen from the Arrhenius plot, these samples from different manufacturers exhibit slightly different conductivities (differing by a factor of ~ 2 at 900 °C), which cannot be solely attributed to the uncertainties in conductivity determination (about 6% at 900 °C). Different defect concentrations in the samples are expected to contribute to this difference.

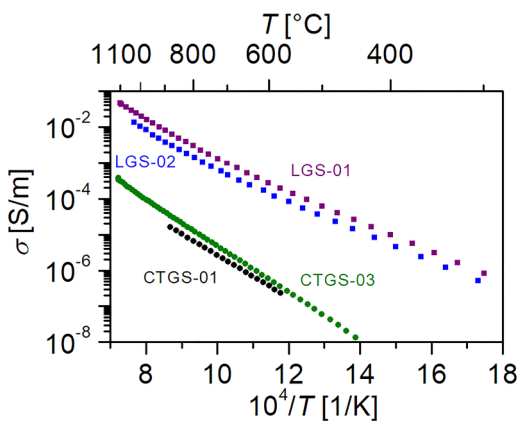


FIG. 2. Conductivities of different LGS and CTGS samples as a function of temperature.

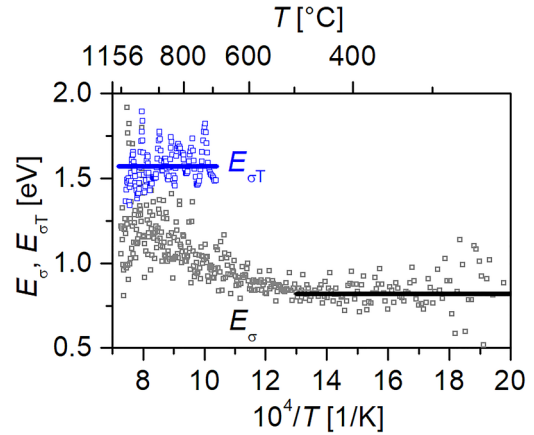


FIG. 3. Slopes E_σ and $E_{\sigma T}$ of the electrical conductivity of LGS-01 (squares) and related ranges of approximately constant derivatives (lines).

The data for these samples are approximately linear as a function of $1/T$ in this semi-log presentation below about 500 °C, indicating that a single thermally activated process determines the conductivity in this temperature range. The appearance of a linear function is supported by an approximately constant slope $E_\sigma = -k_B \partial \ln(\sigma) / \partial(1/T)$ below 500 °C, as indicated by the solid black line for sample LGS-01 in Fig. 3. Here, the derivative $\partial \ln(\sigma) / \partial(1/T)$ is calculated without smoothing (slope from one point to the next) and plotted as gray open squares in Fig. 3. As reported in Ref. 36, electronic conduction governs the conductivity in LGS up to 700 °C [Eq. (8)]. Above about 500 °C, the slope starts to change, which implies that a different process increasingly contributes with increasing temperature. In order to separate this high-temperature contribution, the low-temperature conductivity is extrapolated to the upper end of the measured range and subtracted from the measured data. The approach is illustrated in Fig. 4, where the solid

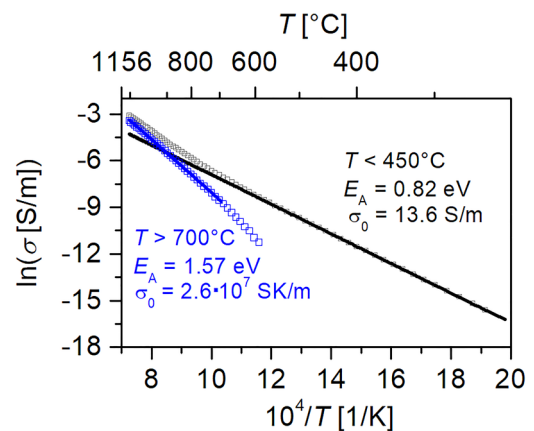


FIG. 4. Electrical conductivity of LGS-01 as measured (squares) with fit and extrapolation of Eq. (8) (gray line) and high-temperature contribution (crosses) and related fit (blue line).

gray line represents a fit of Eq. (8) to the data in the range of 250–500 °C and its extrapolation to 1150 °C. The blue open squares in Fig. 4 show the high-temperature contribution, which is the difference between the measured data and the extrapolated low-temperature contribution.

With increasing temperature, ionic conduction becomes dominant,³⁶ and the corresponding Arrhenius expression has a pre-exponential factor that is inversely proportional to T [Eq. (9)]. Consequently, the related slope $E_{\sigma T}$ is equal to $-k_B \partial \ln(\sigma T) / \partial (1/T)$. The calculation of $E_{\sigma T}$ followed from the difference of measured data and the extrapolated low-temperature data. This difference (Fig. 4) shows a relatively large scatter and was, therefore, smoothed using an FFT algorithm prior to the slope calculation. The result of this calculation is plotted as blue open squares in Fig. 3 from 700 °C to the highest measured temperature and is seen to have no overall temperature dependence. Finally, the activation energy is determined by the fitting of Eq. (9) to the high-temperature contribution. The result is shown as the blue solid line in Fig. 4. The same procedure is applied to the conductivity data from sample LGS-02 (not shown).

The activation energies obtained from separate least-square fits, using the above-described approach are (0.82 ± 0.05) and (1.57 ± 0.07) eV for the LGS-01 specimen for the electronic and ionic conduction mechanisms, respectively. For the LGS-02 sample, the corresponding activation energies are (0.78 ± 0.05) and (1.49 ± 0.07) eV.

The conductivities of samples CTGS-01 and CTGS-03 are also shown in Fig. 2. For both CTGS specimens, only every fifth data point is plotted. As seen from the figure, the conductivity values of CTGS are more than two orders of magnitude lower than those of LGS at 900 °C and about three orders of magnitude lower at 570 °C. Similarly to LGS, the two CTGS samples show slightly different conductivities. Note that variations in conductivity were observed previously even for CTGS samples manufactured from the same boule.³¹

The conductivities of both CTGS specimens increase approximately linearly in the Arrhenius presentation, indicating that they are governed by a single thermally activated process over the entire measured temperature range. Least-squares fitting of the CTGS conductivity data to Eq. (8) yields activation energies $E_A = (1.15 \pm 0.07)$ and (1.24 ± 0.07) eV for the CTGS-01 and CTGS-03 specimens, respectively.

The parameters from the fit for the measured LGS and CTGS samples are listed in Table II.

TABLE II. Parameters obtained from the fits of conductivity of the CTGS and LGS samples.

Sample	Activation energy (eV)	Pre-exponential factor	Temperature range (°C)
LGS-01, LT	0.82 ± 0.05	13.6 S/m	400–700
LGS-01, HT	1.57 ± 0.08	2.58×10^7 SK/m	700–1100
LGS-02, LT	0.78 ± 0.05	4.46 S/m	400–700
LGS-02, HT	1.49 ± 0.07	6.34×10^6 SK/m	700–1050
CTGS-01	1.15 ± 0.07	2.1 S/m	570–900
CTGS-03	1.24 ± 0.07	19.0 S/m	400–1100

B. Loss measurements

1. Langasite

The measured Q^{-1} of the LGS-01 sample is presented in Fig. 5 as a function of inverse temperature. These measurements were performed on the electroded specimen by RPS. The frequency is the first harmonic of the TSM resonator, equal to about 850 kHz at room temperature and decreasing monotonically with heating to 810 MHz at 1100 °C. Reliable measurements were obtained for the temperatures above 350 °C. Below this temperature, a substantial number of sharp peaks that appeared in the raw data for this sample were observed, making correct evaluation of data impossible. Such spikes vs temperature are understood as originating from the “activity dip” phenomenon, which is caused by signal interference and energy loss to “spurious” modes with in-plane phase variation and correspondingly greater components of displacement that are not through-thickness shear.⁵⁵

As shown in Fig. 5, a broad temperature-dependent peak is observed in $Q^{-1}(T)$ between about 400 and 1100 °C. Based on previous studies,^{2,36,38} this attenuation is attributed to anelastic point defect relaxation, superimposed by piezoelectric/carrier relaxation, as derived from conductivity data presented in Sec. IV A. As already mentioned in Sec. III C, two different conduction mechanisms govern the conductivity in LGS. Specifically, ionic and electronic relaxations are expected to contribute to $Q^{-1}(T)$ at elevated temperatures. From the dielectric-constant and conductivity data plotted in Figs. 1 and 2, the dielectric relaxation frequencies $f_c = \omega_c / (2\pi)$, which determine the maxima of conductivity-related contributions, can be calculated using Eq. (6). These calculations predict that f_c is equal to 810 kHz at 741 °C for the electronic conduction mechanism and 809 °C for the ionic conduction mechanism. These predicted temperatures at which each dielectric relaxation frequency matches the resonant frequency

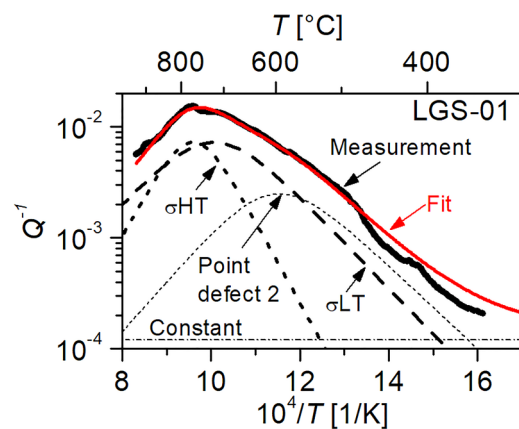


FIG. 5. Measured Q^{-1} of LGS-01 with resonance frequency at 850 kHz as a function of temperature (black symbols), corresponding least-squares fit to Eq. (12) (solid red line), and separate contributions to Q^{-1} (dashed and dotted lines).

correlate well with the measured maximum of the broad peak in Q^{-1} between 700 and 800 °C (Fig. 5).

Equation (12) for $Q^{-1}(T)$ with one anelastic point defect relaxation term ($n = 1$) and two piezoelectric/carrier relaxation terms is fitted to the measured LGS-01 data. Here, the Akhiezer term ($B\omega$) is ignored because it is expected to be insignificant relative to other contributions in this specimen, as discussed in detail in Sec. V B, and it cannot be separated from the constant term C_0 in an analysis of the measurements of a single harmonic. The results of this fit are presented in Fig. 5. Here, σ_{LT} and σ_{HT} correspond to the electronic and ionic piezoelectric/carrier relaxations, respectively. In this analysis, the data points were weighted equally on a logarithmic scale and the measured temperature dependence of the frequency was included. The parameters extracted from this fit are summarized in Table III and discussed in detail in Sec. V. It should be noted that the maxima of the electronic and ionic piezoelectric/carrier relaxations, extracted from the fit, are found at about 720 and 770 °C, respectively. These values are close to the corresponding temperatures predicted from the dielectric relaxation frequencies calculated from the fit parameters of the conductivity data, above.

The measured $Q^{-1}(T)$ of the LGS-02 sample is presented in Fig. 6. Similarly to LGS-01, this specimen with electrodes was studied by RPS. The fundamental frequency of this TSM resonator is 5.43 and 5.18 MHz at room temperature and 1050 °C, respectively.

As seen in Fig. 6, two peaks with maxima near 250 and 650 °C are present in this sample. These peaks do not match the piezoelectric/carrier relaxations expected from conductivity data presented in Refs. 2 and 36. Previously, they were attributed to anelastic point defect relaxations.^{34,36,37} At higher temperatures, the maximum of another peak near 990 °C is observed. This peak has been attributed to piezoelectric/carrier relaxation.^{2,36} Using the parameters from the fits to the conductivity data of LGS-02, the calculation of dielectric relaxation frequencies yields $f_c = 5.2$ MHz at 1019 °C for the ionic conduction mechanism. This prediction is close to the measured peak temperature, and the difference is attributed to uncertainties in measurement, as discussed in Sec. V A.

TABLE III. Fit parameters obtained from the fits of $Q^{-1}(T)$ of the LGS-01 and LGS-02 samples.

	LGS-01	LGS-02
Δ_1	n/a	0.24
γ_1	n/a	2.23×10^{-11} s
E_1	n/a	0.333 eV
Δ_2	4.44	5.38
γ_2	3.71×10^{-12} s	3.10×10^{-12} s
E_2	0.801 eV	0.804 eV
K^2	1.45×10^{-2}	7.02×10^{-3}
γ_c (electronic)	1.27×10^{-11} s	5.46×10^{-11} s
E_c (electronic)	0.821 eV	0.762 eV
γ_c (ionic)	7.94×10^{-18} s/K	3.35×10^{-17} s/K
E_c (ionic)	1.532 eV	1.454 eV
C_0	1.20×10^{-4}	1.00×10^{-4}

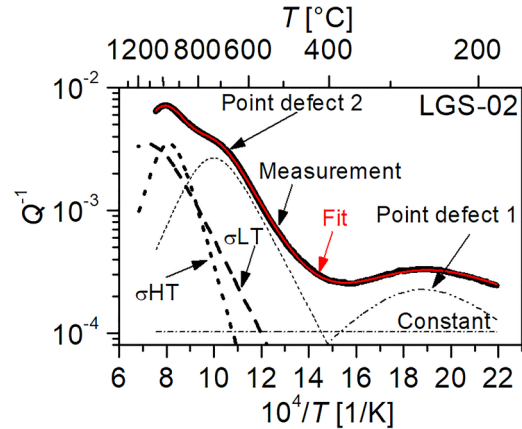


FIG. 6. Measured Q^{-1} of LGS-02 with resonance frequency at 5.4 MHz as a function of temperature (black symbols), corresponding least-squares fit to Eq. (12) (red line), and separate contributions to Q^{-1} .

For the electronic conduction mechanism, it follows that $f_c = 5.2$ MHz at 1157 °C, which is above the highest measured temperature. Nevertheless, the influence of both contributions in the observed maximum is strong.

Expression (12) for $Q^{-1}(T)$ with two point-defect relaxation terms, two piezoelectric/carrier relaxation terms, and a constant background is fitted to the measured LGS-02 data. Similarly, to the fitting of the loss of LGS-01, the phonon-phonon term ($B\omega$) is ignored here, and the temperature dependence of the resonance frequency is considered. The results of the fit are plotted in Fig. 6 and the parameters extracted from this fit are listed in Table III.

2. Catangasite

Measurements of the temperature-dependent Q^{-1} of sample CTGS-02 are presented in Fig. 7. These measurements were

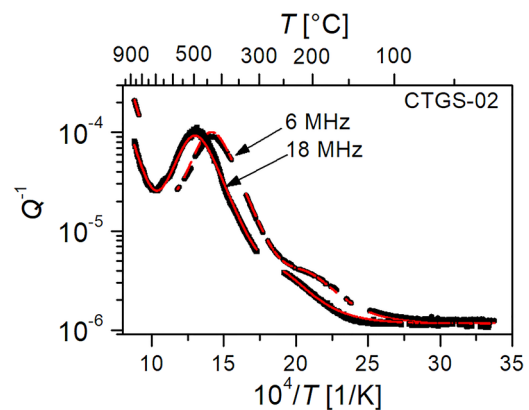


FIG. 7. Measured Q^{-1} of sample CTGS-02 as a function of temperature (black symbols) and multi-frequency fit (red lines) at 6 and 18 MHz.

performed on the sample with non-contacting electrodes and toneburst excitation, as described in Sec. III B. The frequencies indicated in the figure correspond approximately to the first and third harmonics of the thickness-shear resonator at room temperature. A substantial number of sharp peaks that appeared in the raw data for this sample have been deleted in the presentation in Fig. 7. As with LGS-01, these peaks are associated with the “activity dip” phenomenon. The time-domain technique for determining Q^{-1} fails when beats from nearby modes are present in the signal with a period close to the time constant of exponential decay. Sustained interference from multiple modes between 575 and 821 °C at 6 MHz led to an inability to measure Q^{-1} in this range, and, similarly, effective measurements could not be performed over several lower-temperature ranges at 6 and 18 MHz, as indicated in Fig. 7.

A broad peak with a maximum near 490 °C at the third harmonic (18 MHz) is attributed to an anelastic point-defect relaxation because of the general form of its dependence on frequency and temperature. On the low-temperature shoulder of this peak, a smaller peak with maximum near 250 °C is visible. Q^{-1} at the highest measured temperatures (above approximately 750 °C at 18 MHz) increases monotonically with increasing temperature. This increase is interpreted as originating from the piezoelectric/carrier relaxation mechanism. The first harmonic shows similar features in the temperature dependence of Q^{-1} , with the peak maxima and highest-temperature monotonic increase shifted to lower temperatures.

As stated in Sec. IV A, the conductivity in CTGS is governed by a single thermally activated process over the entire measured temperature range. Hence, in contrast to LGS, only one piezoelectric/carrier relaxation mechanism is expected to contribute to $Q^{-1}(T)$. The temperature at which the maximum of this relaxation would occur in CTGS resonators with frequencies in the megahertz range can only be estimated, since it is above the melting temperature of CTGS.

The function in Eq. (12), with two point defect relaxations, a single piezoelectric/carrier relaxation, Akhiezer loss, and a temperature-independent background, was fitted to the measured Q^{-1} of CTGS-02. In this analysis, the data from both harmonics were fitted simultaneously with the temperature dependence of the frequencies included. Since the maximum of the piezoelectric/carrier relaxation lies far above the measurement range (and above the melting point), $\omega\tau_c$ in the piezoelectric/carrier contribution of Q^{-1} [Eq. (7)] is much greater than 1 in the measured temperature range, and the loss is closely approximated as $Q^{-1} = K^2(\omega\tau_c)^{-1} = K^2(\omega\gamma_0)^{-1}\exp(-E_c/kT)$. Since only the ratios of K^2 and γ_0 appear in this expression, these two parameters cannot be separately optimized in the fitting of the data. Therefore, the electromechanical coupling factor K^2 was fixed at the value listed in Table IV (0.031), which is calculated using published values for e_{11} , c_{66} ⁵³ and the average measured ϵ_{11} above 700 °C, 17.14 ϵ_0 (Fig. 1). The curves for the two harmonics determined from this fit are plotted in Fig. 7, and the corresponding fit parameters are listed in Table IV.

The fit parameter B for CTGS-02, associated with phonon-phonon interactions, was found to be zero. This value is not included in Table IV. We note that, based on previous studies of LGS and LGT^{37,56} and the expectation that ordered crystals in the langasite family will not have higher phonon-phonon loss than

TABLE IV. Fit parameters obtained for the $Q^{-1}(T)$ dependences of the CTGS-02 and CTGS-03 specimens.

	CTGS-02	CTGS-03
Δ_1	2.21×10^{-3}	n/a
γ_1	9.55×10^{-14} s	n/a
E_1	0.525 eV	n/a
Δ_2	0.14	0.25
γ_2	4.74×10^{-14} s	4.05×10^{-14} s
E_2	0.810 eV	0.821 eV
Δ_3	n/a	5.42×10^{-2}
γ_3	n/a	2.02×10^{-12} s
E_3	n/a	0.945 eV
K^2	0.031 (fixed)	0.031 (fixed)
γ_c	1.46×10^{-10} s	4.85×10^{-11} s
E_c	0.998 eV	1.240 eV
C_0	1.16×10^{-6}	2.24×10^{-5}

partially disordered crystals, the parameter $B\omega$ is expected to be smaller than the determined value of C_0 . The minor role of phonon-phonon loss over the entire measurement range apparently leads to an inability to extract a realistic value for B .

The contributions to the Q^{-1} of sample CTGS-02 at 18 MHz obtained from the fit to Eq. (12) are shown separately in Fig. 8. As seen in this figure, the loss is dominated by the non-material contribution (C_0 , associated with mounting) in the temperature range up to ~208 °C. Above this temperature, point-defect relaxations (two peaks with maxima at ~270 and ~500 °C) become the dominant mechanisms up to ~695 °C where the contributions from the higher-temperature point-defect relaxation and the piezoelectric/carrier relaxation are equal. At higher temperatures, the piezoelectric/carrier contribution is dominant. Specifically, in the range $10^4/T < 9$, the contribution of the second point-defect relaxation is less than 6% of the piezoelectric/carrier contribution.

The temperature-dependent Q^{-1} of the CTGS-03 sample is shown in Fig. 9 as an Arrhenius plot. Similarly to LGS specimens,

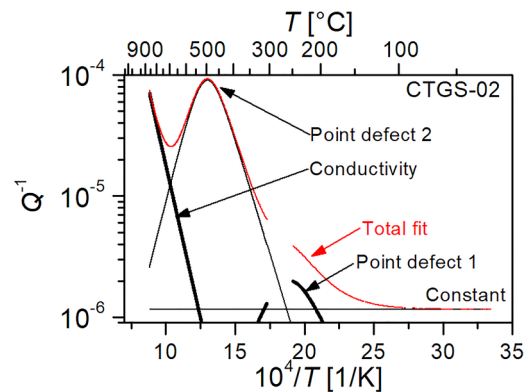


FIG. 8. Separate contributions to Q^{-1} of sample CTGS-02 at 18 MHz.

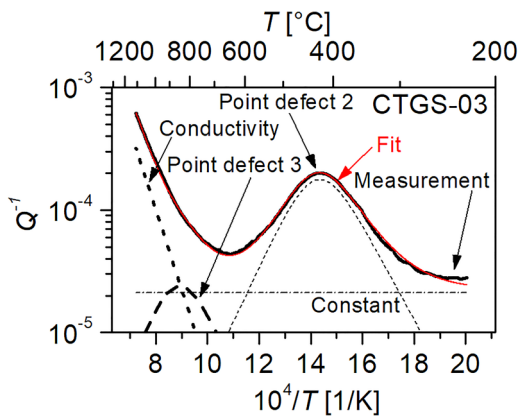


FIG. 9. Measured Q^{-1} of sample CTGS-03 as a function of temperature (black symbols), corresponding least-squares fit to Eq. (12) (red line), and separate contributions to Q^{-1} .

these measurements were performed on the sample with electrodes by RPS. The fundamental frequency of this TSM resonator is 5.00 MHz at RT, monotonically decreasing to 4.78 MHz at 1100 °C. The results in Fig. 9 show a broad peak in $Q^{-1}(T)$ with a maximum at about 420 °C, similarly to the loss in CTGS-02 (Fig. 7). Since the measurements were performed above 225 °C, the maximum of the lowest-temperature peak that is observed in CTGS-02 (Figs. 7 and 8) is not observed for CTGS-03. However, the positive deviation of the data relative to the fit in the range of 225–250 °C is interpreted as the shoulder of that peak. Above 750 °C, a rapid increase in Q^{-1} is observed, similarly to CTGS-02.

Initially, the function in Eq. (12) with one point-defect relaxation and one piezoelectric/carrier relaxation was fitted to the measured Q^{-1} of CTGS-03 (results not given). However, this fit did not closely match the data or provide credible parameters for the piezoelectric/carrier relaxation, considering the associated parameters independently determined from conductivity measurements (Table II; Fig. 2). Since the problems with this fitting function are most pronounced at temperatures above the peak of the point-defect relaxation, a second fit was performed with an assumption that an additional point defect relaxation contributes to the loss above 750 °C. The results of this fit are plotted in Fig. 9 and the fit parameters are summarized in Table IV and discussed in detail in the next section. Note that, similarly to LGS, the Akhiezer term ($B\omega$) is ignored in this fit, since its contribution is expected to be insignificant, relative to other contributions above 200 °C. Furthermore, similarly to CTGS-02, the electromechanical coupling factor K^2 was approximated as a constant for the fit procedure with $K^2 = 0.031$.

3. Comparison of CTGS, LGS, and LGT

In Fig. 10, the measured $Q^{-1}(T)$ of the LGS and CTGS resonators are compared with those of LGT, obtained and analyzed previously.³⁷ In this figure, the constant fit term C_0 was subtracted from the data to enable an effective comparison of the material

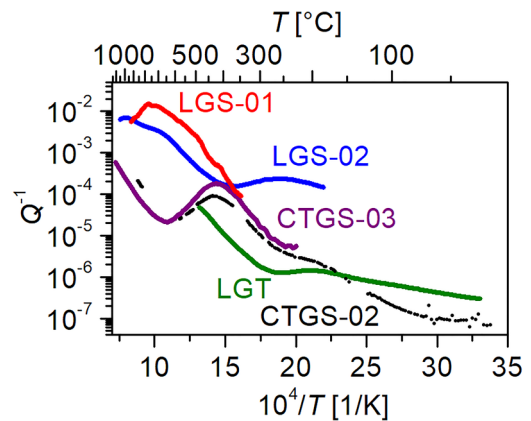


FIG. 10. Measured Q^{-1} of the LGS-01 (850 kHz), LGS-02 (5 MHz), CTGS-02 (6 MHz), CTGS-03 (5 MHz), and LGT (6 MHz) samples as a function of temperature, with constant C_0 from the fit of the measurements of each specimen subtracted.

contributions. As seen in this figure, the material loss in LGS at 5 MHz (LGS-02) is substantially higher than that in CTGS and LGT at similar frequencies over the entire measured temperature range. In particular, the difference between measured losses in the LGS-02 and CTGS-02 resonators at 200 °C is almost two orders of magnitude. The LGT specimen shows the lowest loss among the studied resonators in the range of about 150–500 °C, which may be attributed to the fact that the LGT resonator has a plano-convex, rather than a plano-plano, surface and, therefore, has more effective trapping of vibrations away from the points of mechanical support.

V. DISCUSSION

A. Conductivity-related loss

The existence of an attenuation peak governed by the conductivity-related mechanism was predicted in Ref. 37 for LGS and LGT, following the general theory of Hutson and White.⁵² However, the measurements in that study did not extend to a temperature range where this mechanism contributed significantly to the loss. Considering the measured temperature-dependent electrical conductivity (Fig. 2) and the studies of LGS performed in Refs. 2, 36, 54, and 57, two independent piezoelectric/carrier relaxations, determined as electronic and ionic, must contribute to $Q^{-1}(T)$. Both piezoelectric/carrier relaxations should have the same relaxation strength, according to the theory of Hutson and White.⁵² Using the measured temperature-dependent dielectric constant (Fig. 1) and conductivity (Fig. 2) for the 850 kHz LGS-01 resonator, the temperatures of the $Q^{-1}(T)$ peak maxima are predicted to be 741 and 809 °C [Eq. (6)], consistent with the maxima of these contributions near 720 and 770 °C determined from the fit of $Q^{-1}(T)$. The differences in these temperatures can be already explained by a combination of the measurement uncertainty for the temperature (1%) and the dielectric constant (10%), without including other uncertainties. The activation energies for the ionic and electronic conductivity-related relaxation mechanisms are found from the fit

of $Q^{-1}(T)$ to be ~ 1.53 and 0.82 eV, which is consistent with the activation energy determined from the bulk conductivity (Table II).

The electromechanical coupling coefficient K^2 for the LGS-01 specimen was determined from the fit of $Q^{-1}(T)$ to be about 0.0145 (Table III). A calculation of K^2 using the values for e_{11} and of C_{66} from Ref. 58 and the measured value of ϵ_{11} (Fig. 1) yields a value of 0.0177 , which is about 1.2 times greater. This 20% difference between predicted and fit values can be attributed to differences in the conductivities of the studied samples and/or uncertainty in the determination of the piezoelectric coefficient at elevated temperatures. The same applies to the values of γ_c extracted from the fits of conductivity and Q^{-1} of LGS-01 [Table II; Table III; Eqs. (10) and (11)].

Because of the frequency dependence of piezoelectric/carrier relaxations [Eq. (7)], their peak maxima at 5 MHz in LGS-02 is shifted to higher temperatures, relative to LGS-01. As in LGS-01, both the ionic and the electronic conduction mechanisms are expected to contribute to $Q^{-1}(T)$ in LGS-02. Inserting the values of dielectric constant and conductivity into Eq. (6), the temperatures of the loss maxima of the piezo/carrier contributions are predicted to be 1019 and 1157 °C at 5.2 MHz (the resonant frequency near 1000 °C) for the ionic and electronic relaxations, respectively. The maxima of these contributions determined from the fit of measured $Q^{-1}(T)$ are 970 and 1125 °C, respectively, consistent with the conductivity measurements, within the uncertainties associated with temperature and the piezoelectric constant. Note that the measurements of LGS-02 are performed only up to 1050 °C; therefore, the predicted maximum of the electronic piezoelectric/carrier loss lies beyond the measured range.

As with LGS-01, the values of E_c and γ_c determined from Q^{-1} and predicted by the measured conductivity and published values of the piezoelectric and elastic constants are consistent within the stated uncertainties [Table II; Table III; Eqs. (10) and (11)]. However, the value of K^2 determined from the fit of Q^{-1} is 0.007 , which is 2.5 times smaller than the expected value of 0.0177 . This difference may primarily arise from an inaccuracy of the assumed piezoelectric constant e_{11} . Since K^2 is proportional to the square of e_{11} , it is especially sensitive to specimen-dependent variations in this material property.

Overall, despite the discrepancy in the estimated and fit K^2 of LGS-02, the close agreement of all fit piezoelectric/carrier relaxation parameters of LGS-01 and γ_c and E_c of LGS-02 with estimates of these parameters based on the measured conductivities and published values of e_{11} provides compelling evidence that the loss contributions associated with both electronic and ionic conduction have been correctly identified in both these specimens. These contributions are shown to dominate the loss at the highest measured temperatures in both specimens.

An additional striking feature of the conductivity and loss of the LGS specimens is the similarity of the activation energies determined for peak 2 (Table III) and the electronic piezoelectric/carrier relaxation (Table II; Table III). Hirschle and Scheuer³⁸ suggested that identical activation energies might arise from piezoelectric/carrier and point-defect relaxations involving the same atomic jump mechanism. Although this may be possible for the ionic conduction mechanism, we find the similarity of activation energies in LGS to be associated with the electronic conduction. Therefore, we

interpret the similarity of the values of activation energy of peak 2 and the electronic conductivity to be a coincidence.

Hirschle and Schreuer³⁸ observed high loss between 330 and 950 °C in LGS at frequencies between 168 and 524 kHz and suggested that this loss arises from either a combination of two different point defect relaxations or a combination of a point defect relaxation and a piezoelectric/carrier relaxation. The temperature range of high loss at these frequencies is consistent with the parameters extracted here for peak 2 and both piezoelectric/carrier relaxations in LGS-01 and LGS-02 (Table III). For example, the fit parameters for Q^{-1} of LGS-02 predict that if this crystal had been fabricated as a 343 kHz resonator, peak 2 would appear at 510 °C, and the electronic and ionic piezoelectric/carrier peaks would appear at 704 and 755 °C, respectively. The fit parameters obtained by Hirschle and Schreuer, under the assumption of two peaks in this temperature range, correspond to peaks at 569 and 731 °C at 343 kHz. Based on our results from LGS-01 and LGS-02, we expect that there are actually three relaxations involved in the loss that Hirschle and Schreuer observe in LGS above 300 °C. Specifically, the fact that the maximum of their highest-temperature peak at 343 kHz is between the peak temperatures predicted for the electronic and ionic relaxations from the LGS-02 fit parameters supports a hypothesis that this peak observed by Hirschle and Schreuer is a superposition of the two piezo/carrier peaks and the second-highest-temperature peak in their measurements corresponds to point-defect peak 2 in our measurements. This correspondence of peak 2 is discussed further in Sec. V B 2.

To further explore the temperature and frequency dependence of the piezoelectric/carrier relaxations, the temperature-dependent dielectric relaxation frequencies f_c of the LGS and CTGS samples are calculated with Eq. (6) and compared in Fig. 11. In this figure, the thin nearly horizontal lines represent the resonant frequencies f_s of the samples and the more strongly temperature-dependent

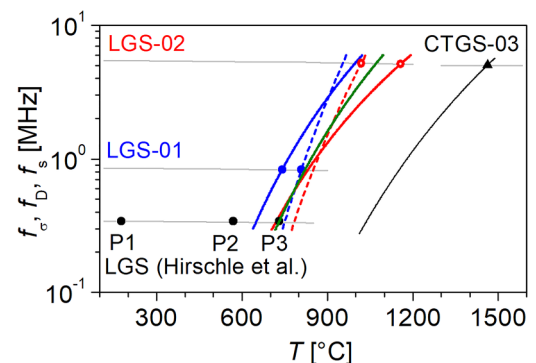


FIG. 11. Dielectric relaxation frequencies f_c , calculated for specimens LGS-01 (red lines), LGS-02 (blue lines), and CTGS-03 (black line) and comparison with peak positions for an LGS specimen given in Ref. 38 (black points). The solid and dashed lines for LGS-01 and LGS-02 represent electronic and ionic conduction mechanisms, respectively. The thin gray horizontal lines are the measured resonant frequencies f_s of the indicated specimens. The green line represents frequency f_D calculated from the fit parameters given in Ref. 38 (see text).

curves are the dielectric relaxation frequencies calculated from the measured conductivities and dielectric constants (Figs. 1 and 2) along with the published values of piezoelectric constants.^{53,58} The intersections of the curves for f_c and f_s are marked by circles and triangles for LGS and CTGS, respectively. Electronic contributions of the samples LGS-01 and LGS-02 are shown as solid red and blue lines, respectively, and ionic contributions are shown as dashed red and blue lines, respectively.

The curves for the electronic f_c of LGS-01 and LGS-02 in Fig. 11 have a similar shape, with the horizontal shift of the curves arising primarily from the difference in the prefactor σ_0 of the conductivity. The shapes of the curves for the ionic f_c of these two samples are also similar to each other, with slopes that are greater than those of the curves for the electronic f_c . The greater slopes are a reflection of the greater activation energies (Table II). Because of the difference in slopes, the curves for the electronic f_c and ionic f_c cross. The dielectric frequency where this crossing occurs is equal to the operating frequency at which the maxima of the two peaks occur at the same temperature, making them, therefore, very difficult to analyze. Separation of the peaks can be achieved by choosing the operating frequency lower or higher than the value of f_c at the crossover temperature. For LGS-01, the value of f_c at the crossover is close to 3 MHz. Therefore, if the resonant frequency is lower than 3 MHz, the peak of the electronic relaxation will occur below that of the ionic relaxation, and, if it is higher than 3 MHz, the temperature ordering of the peaks will be reversed. Regardless of the resonant frequency, the loss from the electronic and ionic contributions will be equal (although not generally maximal) at the temperature where the two f_c curves cross, because the relaxation strengths of the two contributions are the same (Sec. III C 3). For both LGS-01 and LGS-02 at any resonant frequency, the electronic contribution is greater than the ionic contribution below a certain temperature because of a lower activation energy.

Furthermore, the dielectric relaxation frequencies are compared with the data of Hirschle and Schreuer for LGS.³⁸ In particular, three loss peaks at a resonance frequency of about 343 kHz are considered [see Fig. 4(a) in].³⁸ These peaks are found at positions marked as P1, P2, and P3 in Fig. 11 from the Debye-function fit parameters given in Table II in Ref. 38. As mentioned above, the positions of peaks P1 and P2 are consistent with point-defect relaxations and are discussed in Sec. V B. For P3, the frequency f_D at which the loss is maximal at a given temperature is calculated from the fit parameters of Hirschle and Schreuer and plotted in Fig. 11 as a green line. The overall slope of this curve is between that of the electronic and ionic curves of LGS-02 in Fig. 11, which supports the hypothesis, presented above, that this peak is a superposition of the two piezoelectric/carrier relaxations.

As indicated in Fig. 11, the maximum of the (electronic) piezoelectric/carrier loss for 5 MHz CTGS resonators is expected to be above 1400 °C (greater than the melting temperature), since the conductivity of CTGS is at least two orders of magnitude lower than that of LGS (Fig. 2). Nevertheless, as with LGS, piezoelectric/carrier relaxation is found to be the dominant loss mechanism in both CTGS-02 and CTGS-03 at the highest measurement temperatures (above ~695 °C in CTGS-02 and above ~850 °C in CTGS-03). The fit of $Q^{-1}(T)$ of CTGS-02, with K^2 fixed at a value predicted from the independently measured dielectric constant of

CTGS-01 (Fig. 1) and piezoelectric constants previously measured with a specimen from a different manufacturer⁵³, has provided values for the piezoelectric/carrier activation energy and pre-exponential time constant (Table IV) that are, respectively, within 0.15 eV and a factor of two of values determined from the fit of the measured conductivity (Table II). These values from the two fits are in reasonable agreement, especially considering the likely differences in conductivity between specimens. For CTGS-03, the fit was performed with the assumption that the increase in loss above 750 °C is a superposition of a piezoelectric/carrier relaxation and an additional point-defect relaxation. The activation energy for the piezoelectric carrier relaxation extracted from this fit is 1.24 eV, matching the value determined from the conductivity measurements. The relaxation time γ_c determined from Q^{-1} is, however, about 6 times greater than that predicted from the measurements of conductivity and ϵ_{11} . We assume that this difference arises primarily from uncertainties in conductivity associated with inhomogeneity of the crystal boule from which the specimens were cut.³¹

B. Point defect relaxations

1. Peak 1

The existence of a loss peak in LGS with a maximum in the range of 250–280 °C at 5 MHz was shown in previous studies of Y-cut resonators.^{34–37} Johnson *et al.*^{34,37} determined an activation energy of 0.538 eV and pre-exponential time constant of 3.72×10^{-13} s from a simultaneous fitting of $Q^{-1}(T)$ of four harmonics of an LGS resonator under the assumption of a Debye function for the dependence on temperature and frequency. In that study, the peak was attributed to anelastic relaxation of point defects on the basis of the compatibility of the measured $Q^{-1}(T)$ with the Debye form and the magnitudes of the activation energy and pre-exponential factor of the relaxation time. From the fit parameters reported in that study, the peak temperature is predicted to be 199 and 272 °C at 850 kHz and 5 MHz, respectively. We note that the measurements of the LGS-01 specimen performed here begin at about 350 °C; therefore, the low-temperature anelastic peak is not visible. The maximum of the lowest-temperature peak in the 5 MHz resonator LGS-02, determined here for LGS-02 from the fit parameters in Table III, is ~259 °C, close to the prediction of 272 °C. However, the values for E_1 and γ_1 , 0.33 eV and 2.23×10^{-11} s, respectively, (Table III) are not in close agreement with the values reported in Ref. 37. We note that the parameters extracted here from data at one harmonic of the LGS-02 specimen may have greater uncertainty than those obtained from measurements at multiple harmonics in Ref. 37. However, as discussed below, different defects may be responsible for the peaks observed between 250 and 280 °C in these two studies of LGS. Note that the values of E_1 and γ_1 obtained here for peak 1 in LGS-02 (Table III) are close to values previously reported for the lowest-temperature peak in LGT (6 MHz data plotted in Fig. 7): 0.292 eV and 1.89×10^{-11} s.³⁷

In resonant ultrasound spectroscopy (RUS) measurements of LGS parallelepipeds at lower frequencies, Hirschle and Schreuer³⁸ observed a small peak during cooling (that may correspond to peak 1 in this study) and speculated that this peak involves point-defect relaxations at the tetrahedrally coordinated position of silicon in

the lattice. They reported an activation energy of $0.4(3)$ eV and a pre-exponential factor of $2(21) \times 10^{-11}$ (where numbers in parentheses are uncertainties in the last digit). This pair of values lies between those listed in Table III for LGS-02 and in Ref. 37 and are consistent with both sets of results, considering the stated uncertainties. They correspond to a peak maximum near 189°C for the measured RUS mode at 343 kHz. From the parameters in Table III, a peak at this frequency is expected to occur near 1116°C at 343 kHz, and, from the parameters reported in Ref. 37, it is expected to occur near 172°C .

Fritze *et al.*³⁵ found that peak 1 in LGS is essentially eliminated by doping with strontium at a concentration equal to 0.25 at. % of the stoichiometric lanthanum concentration in LGS. These authors proposed that strontium (Sr^{2+}) replaces lanthanum (La^{3+}) at the A-site, thereby acting as an acceptor, and charge compensation can then occur through a loss of oxygen from the crystal and the associated generation of doubly charged oxygen vacancies. Note that, following this physical model, peak 1 can be attributed to neither doubly charged oxygen vacancies nor any defect involving Sr, since the peak height is found to decrease with increasing concentrations of both of these types of defects. One potential explanation of the dependence on Sr doping is that peak 1 arises from a defect that undergoes a change in symmetry and the associated relaxation strength with the introduction of Sr because of a change in the charge state of the defect. The dependence of defect symmetry on charge state can arise from the Jahn–Teller effect, which links electronic orbital degeneracy of a defect to vibronic-state orientational degeneracy.⁵¹ We find few published reports of indirect dependence of peaks on doping and associated changes in defect charge and symmetry. However, dopant dependence of the relaxation strength of a peak in bismuth germanium oxide, $\text{Bi}_{12}\text{GeO}_{20}$ (BGO), has been attributed to charge-related changes in symmetry of an unidentified anelastic defect.⁵⁹ Zn doping of the high-temperature superconductor $\text{YBa}_2\text{Cu}_3\text{O}_{6+\delta}$ (YBCO) is reported to reduce the height of a relaxation peak, and this effect is attributed to a change in the charge distribution and the associated Jahn–Teller distortion of oxygen localized near Zn (which substitutes for Cu in the lattice), even though Zn does not act as a global acceptor or donor.^{60,61}

The measurements of CTGS-03 indicate the possible presence of a relaxation with a maximum below the temperature range of the measurements (with a lower limit of 225°C), as described in Sec. IV B 2. In CTGS-02, a peak near 215°C is observed at 6 MHz (Fig. 7). The temperature of this peak maximum is substantially different than the value of 83°C (at 6 MHz) previously reported for a CTGS crystal from a different source,³⁹ and the activation energy of (0.515 ± 0.005) eV found here for CTGS-02 is also different than the value of (0.315 ± 0.005) eV reported in that previous study. Note that the measurements of $Q^{-1}(T)$ of these two specimens were performed with the same experimental system. The differences in these results indicate that two distinct point-defect species can contribute to acoustic loss in the low megahertz range in nominally undoped CTGS below 300°C .

The difference in activation energies from these two sets of data from CTGS crystals is strikingly similar to that obtained for peak 2 in LGS crystals in this study and Ref. 37 (described above), although the difference in the temperatures of the LGS peak

maxima is not as great as that in the two sets of CTGS data. This leads us to suggest that two defect species can also contribute to acoustic loss in nominally undoped LGS below 300°C . A similar situation seems likely to exist in LGT, especially considering how closely the reported activation energy of 0.292 eV of a peak in LGT³⁷ matches the activation energies obtained here for LGS and previously reported for CTGS.³⁹

2. Peak 2

Anelastic peaks similar to peak 2 in LGS-01 (with a maximum near 575°C , Fig. 5) have previously been reported in LGS, LGT, and CTGS.^{33–38} Johnson *et al.*,³⁷ reported a point defect relaxation in LGS with an activation energy of 0.87 eV and time constant of 1.8×10^{-13} s, close to the values found here for peak 2 in LGS-01 and LGS-02 (Table III), even though the temperature range of that study did not include the peak maximum. That previous study also reported values of 0.849 eV and 1.31×10^{-13} s for a relaxation in LGT, and the similarity of these values to those found here for both LGS samples (Table III) supports the hypothesis that a similar defect is responsible for this relaxation in LGT.

As already mentioned in Sec. V A, Hirschle and Schreuer³⁸ found a peak in LGS with a maximum at 569°C at 343 kHz, under the assumption that two peaks are superimposed above 300°C . This peak temperature is not greatly different from temperatures of 519 and 510°C at 343 kHz predicted from the fit parameters for LGS-01 and LGS-02, respectively (Table III). The activation energy obtained by Hirschle and Schreuer for this relaxation is (0.75 ± 0.02) eV.

The activation energies and relaxation times for peak 2, determined from the separate fits of LGS-01 and LGS-02, are found to be very close. In order to confirm the same origin of peak 2, we have calculated the peak temperatures for the frequencies of LGS-01, using the fit parameters of LGS-02 and compared them with the peak position of LGS-01. The latter correspond to the measured values (see Fig. 5). An example of this calculation is shown in Fig. 12. The frequency corresponds to the fundamental frequency of LGS-01 (~ 850 kHz) and the temperature shift of the resonance frequency is considered. As seen from Fig. 12, the positions of the maximum are very close to the same (575°C for LGS-01 and 567°C for LGS-02), which indicates that the same physical mechanism is responsible for peak 2 in both LGS specimens.

Following Johnson *et al.*,^{34,37} we interpret this peak as a point defect relaxation. The relaxation strength is in the typical range of point defect relaxations with defect concentrations on the order of 10 ppm.^{46,62} Because of the closeness of the activation energies of this point-defect relaxation and the conductivity below 700°C , one might suppose that this relaxation and the conductivity involve the same type of atomic jumps. However, this hypothesis is not viable, because the dominant conduction mechanism below 700°C has been shown to be electronic, rather than ionic.³⁶

For both CTGS-02 and CTGS-03, the values determined here for the activation energy (0.81 and 0.82 eV, respectively) and the pre-exponential factor (4.74×10^{-14} and 4.05×10^{-14} s) of peak 2 (Table IV) are close to values reported by Suhak *et al.*^{39,42} for a CTGS crystal from a different source (Institute for Crystal Growth, Berlin, Germany). This peak is the dominant contribution to the

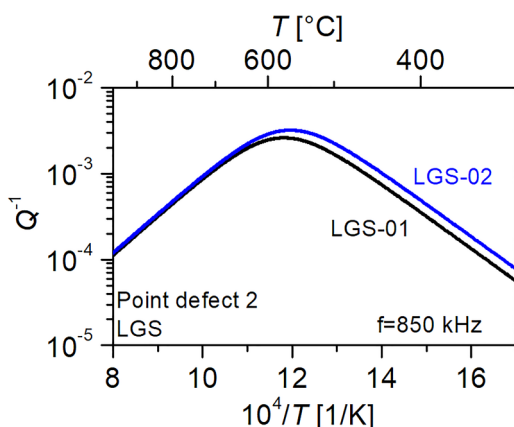


FIG. 12. Calculated peak maxima at 850 kHz using the fit parameters for LGS-01 and LGS-02 (see text for details).

loss in both studied CTGS specimens between 280 and 710 °C (Figs. 7–9). Similar peaks were also previously reported by Johnson *et al.*^{40,41} for Y-cut and singly rotated CTGS resonators and they were attributed to point-defect relaxations.

Note that the activation energies determined for peak 2 in CTGS-02 and CTGS-03 (Table IV) are very close to those for peak 2 in LGS (Table III). However, the pre-exponential factors differ by more than one order of magnitude. Therefore, despite the qualitative similarity of the peaks in these two materials, a hypothesis that they arise from the same types of defects is not supported by these data.

Similarly to LGS specimens, we have performed the calculations of the peak 2 temperatures with the fit parameters of CTGS-02 and CTGS-03 at a frequency of CTGS-03 (Fig. 13). As with LGS, the obtained results clearly indicate that the attenuation at about 430 °C at 6 MHz originates from the same physical

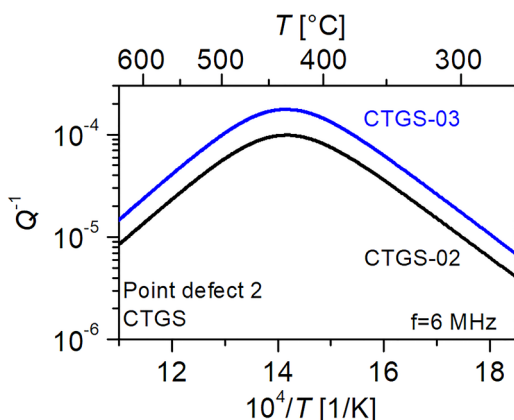


FIG. 13. Calculated peak maxima at 6 MHz using the fit parameters for CTGS-02 and CTGS-03 (see text for details).

mechanism. Here, the temperature shift is even smaller and equals about 2 K.

3. Peak 3

The existence of another point defect relaxation that contributes significantly to the overall loss above 750 °C in CTGS-03 is suggested as a possible explanation for the inconsistency in parameters for piezoelectric/carrier relaxation determined from an initial fit of $Q^{-1}(T)$ and associated parameters determined from conductivity measurements (Table II). Similar inconsistencies were observed in our previous studies of acoustic loss in CTGS^{39,42} and LGS.^{34,37} In these works, expressions for the temperature-dependent background that increases monotonically with the temperature^{34,37,39,42} or a superposition of relaxations with a broad distribution of activation energies^{34,37} were introduced to improve fits at the highest temperatures. The physical mechanisms of such a temperature-dependent background remain unclear. However, it was suggested for LGS in Ref. 37 that it could be associated with a dislocation kink migration mechanism. In the current study, the third peak in CTGS-03 plays a similar role, and its origin (point defects) is clearer with respect to the physical interpretation. Although the uncertainty in the fit parameters for this peak is relatively large, these parameters are consistent with the typical values reported for relaxations of point defects.⁵¹

If this hypothesis of the presence of a third point-defect relaxation is correct, the fit provides evidence that the relaxation has a maximum near 847 °C, and has the most pronounced contribution to the overall Q^{-1} in CTGS-03, operated near 5 MHz, in a very narrow temperature range between 800 and 840 °C. The contribution in this range is nearly equal to those from the piezoelectric/carrier relaxation and temperature-independent background (Fig. 9).

The operating frequencies of CTGS-02 are higher and the maximum of peak 3 is expected to be at 868 and 1010 °C for 6 and 18 MHz, respectively, assuming the same activation energy and pre-exponential factor as determined from the fit of CTGS-03. Since the measurements of CTGS-02 extended only to 860 °C and the data for the temperatures between 580 and 820 °C were missing for 6 MHz, this could potentially explain why no clear evidence of this relaxation was found for the CTGS-02 specimen. However, especially considering that the extracted piezoelectric/carrier activation energy of 0.998 eV for CTGS-02 (Table IV) was lower than that expected from the conductivity data of both CTGS-01 and CTGS-03 (Table II) and lower than that determined from the fit of Q^{-1} of CTGS-03 (Table IV), the loss at the highest temperatures in CTGS-02 could be a superposition of the piezoelectric/carrier relaxation and a third point-defect peak with a lower activation energy similar to that found for peak 3 in CTGS-03.

C. Akhiezer damping and contact loss

Intrinsic Akhiezer (phonon–phonon) loss often serves as the limiting factor for Q in high-quality piezoelectric crystals with effective vibrational trapping at temperatures below ~ 100 °C and frequencies in the low megahertz range. Since this loss is approximately proportional to frequency in this range, it is convenient, when compared with resonators, to consider the Qf product, which

is approximately constant for a given crystal at megahertz frequencies, if Akhiezer loss is dominant.

Smythe *et al.*⁵⁶ found the highest Qf product of a set of unplated plano-convex LGS resonators to be approximately 1.3×10^{13} Hz, corresponding to a value of 3.8×10^{-7} for the intrinsic Akhiezer Q^{-1} at 5 MHz. Since this value of Q^{-1} is almost three orders of magnitude smaller than the lowest values of Q^{-1} in LGS-01 and LGS-02 (Figs. 5 and 6), Akhiezer loss has not been included in the fitting of these data. Similarly, the minimal measured loss in CTGS-03 is approximately two orders of magnitude greater than the expected range of Akhiezer loss⁶³ and, therefore, is not considered in the fit. The only specimen in this study for which the measured loss approaches the expected range of Akhiezer loss is CTGS-02. However, with this loss term included in the fit of the loss of this specimen, the optimized output sets B to zero. This result is qualitatively similar to that obtained by Johnson *et al.*³⁷ from a fit of the loss of an LGS specimen where the extracted Akhiezer factor B was not zero but still unrealistically small. These authors pointed out that an accurate determination of B will be confounded in the presence of substantial contact loss, because contact loss is not actually frequency independent (as approximated by the constant term C_0). As reflected, for example, in the frequency dependence of Qf products for plano-convex LGS, LGN, and LGT measured by Smythe *et al.*,⁵⁶ contact loss is generally higher at lower frequencies, due to less efficient vibrational trapping. Therefore, the assumption of frequency independence of C_0 will lead to a reduction in the magnitude of the Akhiezer term extracted from a fit of Q^{-1} . This explanation for the unrealistic value of zero determined for B in the fit of the CTGS-02 loss is supported by the signs of the deviations of the fit from the data at the two harmonics shown in Fig. 7: the data are above the fit at 6 MHz and below the fit at 18 MHz, consistent with a higher contact loss at a lower frequency. Specifically, the average ratio of the Q^{-1} at 6 MHz to that at 18 MHz at temperatures below 80 °C is 1.15, consistent with a frequency dependence of approximately $1/f^{-0.12}$.

The situation with CTGS-02 is different than that found for the LGT sample,³⁷ which was measured with the same experimental system at the NIST but found to have a contact loss that was an order of magnitude smaller than the Akhiezer loss at 10 MHz. The substantial difference in these results may be attributed to the fact that the LGT resonator has a plano-convex, rather than a plano-plano, surface and, therefore, has more effective trapping of vibrations away from the points of mechanical support. In both the CTGS-02 and the LGT samples, the losses associated with mechanical contact and phonon-phonon interactions play minor roles at elevated temperatures, where the relaxations of point defects and/or piezoelectric/carrier relaxation are dominant.^{46,47,49}

D. Overall losses of different samples

Reported acoustic loss of LGS resonators at ambient and elevated temperatures is generally higher than that of other crystals of the langasite family.^{37,40,56} The measured $Q^{-1}(T)$ of LGS-02 specimen in this study is, however, almost an order of magnitude greater in the range of 200–500 °C than in the data reported in Refs. 33 and 37, which were acquired with noncontacting electrodes and relatively little mechanical contact. The differences in measured

losses could be associated with greater mechanical contact and/or platinum electrodes that were used for measuring this LGS specimen in the current study. The constant terms extracted from the fit of the LGS-01 loss is two orders of magnitude greater than that obtained for the CTGS-02 crystal, which were measured with non-contacting electrodes.

The LGS-01 shows the highest losses among all the studied samples. We note, however, that the influence of piezoelectric/carrier relaxations, superimposed with the point defect relaxation, is significant in the measured temperature range of LGS-01, as discussed above. Furthermore, the electrodes on platinum LGS-01 and the mechanical contact are also expected to contribute to the overall loss, similarly to LGS-02.

Further, a temperature analysis of Q^{-1} in LGS-02 reveals relatively high defect-related loss contributions in the range of 200–450 °C, compared with other samples in this study, as reflected in the much greater relaxation strength, Δ_1 of LGS-02 in Table III. However, note that this will not necessarily be the case for all LGS samples, since, as shown in Ref. 35, peak 1 can be eliminated by Sr doping.

The overall loss of both CTGS specimens has a temperature dependence similar to that reported in previous studies.^{31,39–42,64} The conductivity-related loss is much less than that in LGS, and the primary point-defect relaxation below 800 °C has a maximum between the temperatures of the point-defect peaks in LGS and LGT.

The LGT resonator has the lowest $Q^{-1}(T)$ of the samples in this study in the range of 160–485 °C and the lowest value of the fit parameter C_0 . The lower value of C_0 is consistent with the plano-convex contour of this resonator effectively reducing the vibrational amplitude at the contact points near the edge.

VI. CONCLUSIONS

The temperature-dependent Q^{-1} was studied in structurally ordered catangasite and partially disordered langasite and compared with our results previously reported for langatate and data on langasite reported by other researchers.

The measurements and analysis of data from the langasite specimen LGS-01 with fundamental frequency near 850 kHz revealed a broadly temperature-dependent loss between 400 and 1100 °C, which is attributed primarily to a superposition of a point-defect relaxation and two independent piezoelectric/carrier relaxations that arise from ionic and electronic conduction mechanisms. These peaks are superimposed on a contribution associated with mechanical contact and electrodes, approximated in the analysis as independent of temperature and frequency. The maxima of conductivity-related losses at about 720 and 770 °C are also expected from independent measurements of the conductivity and dielectric constant. The activation energies and the pre-exponential relaxation times of the piezoelectric/carrier relaxations and conductivity are found to be close to the same, and the piezoelectric/carrier relaxation strength is also found to be consistent with an estimate based on the measured dielectric constant and previously reported piezoelectric and elastic constants.

As in LGS-01, a point defect relaxation peak and two piezoelectric/carrier relaxation peaks are observed in the $Q^{-1}(T)$ of

LGS-02. Since the fundamental frequency of this specimen is 5.4 MHz (at room temperature), all three peaks are shifted toward higher temperatures. For the point-defect relaxation, the activation energy, pre-exponential constant, and relaxation strength are found to be close to those determined for LGS-01, indicating similar densities of the defect species responsible for this relaxation. For the piezoelectric/carrier relaxations, the fit activation energies, relaxation times, and corresponding temperatures of the peak maxima are close to those predicted from conductivity measurements. The fit relaxation strength of piezoelectric/carrier relaxations is, however, found to be 2.5 times lower than that predicted from dielectric, piezoelectric, and elastic constants. This difference is attributed primarily to uncertainty in the piezoelectric coefficient.

In both studied CTGS specimens, a peak in $Q^{-1}(T)$ with a maximum between 400 and 500 °C is observed at frequencies between 5 and 18 MHz. In CTGS-02, a much smaller peak with a maximum near 250 °C is also present. This lower-temperature peak is not apparent in CTGS-03, since the measurements of this specimen were performed only above 225 °C. The general form of peaks and their dependence on frequency and temperature leads to the conclusion that the source of these peaks is defect-related relaxations. The rapid increase in loss above 650 °C for both CTGS specimens is interpreted as originating primarily from piezoelectric/carrier relaxation. The maximum of this contribution, calculated from the conductivity measurements, is expected to lie above the melting point of CTGS. For CTGS-03, the inclusion of an additional point-defect relaxation with a fit maximum at about 847 °C led to more credible extracted parameters for the piezoelectric/carrier contribution to $Q^{-1}(T)$. For CTGS-02, the maximum of this third peak is expected to occur just above the measured temperature range, so that extraction of parameters for this potential peak separately from those of the piezoelectric/carrier relaxation parameters is impractical.

The constant contributions to the fits of Q^{-1} are found to be much smaller for measurements of CTGS-02 with noncontacting electrodes than for measurements of CTGS-03, LGS-01, and LGS-02 with deposited platinum electrodes. The greater contributions of this type in measurements with contacting electrodes is interpreted here as arising primarily from the radiation of acoustic energy into the electrical leads and supporting structure. However, anelastic loss in the platinum may also be significant.

With the constant fit term subtracted from the data from each specimen, the loss in the CTGS specimens measured at both the NIST and the Clausthal University of Technology is found to be much less than that in both LGS specimens at all measured temperatures, except for a small temperature range near the maximum of the largest point-defect peak in CTGS (near 430 °C). The greater loss in LGS at higher temperatures is due to a combination of a higher conductivity and the presence of a point-defect peak with a relaxation strength more than an order of magnitude greater than the largest point-defect peak observed in CTGS. Similarly, high loss in LGS-02 below 400 °C is attributed to a point-defect peak with a relaxation strength that is two orders of magnitude greater than that of a point-defect peak in CTGS-02 in this temperature range. While one might be tempted to conclude from these results that the greater loss in LGS, relative to CTGS, is generally associated with the partially disordered crystal structure of LGS, this broad conclusion is not supported by a comparison of the CTGS loss

with that of LGT, which is also a disordered crystal. The measured loss of the LGT specimen at intermediate temperatures (from 160 to 485 °C) is lower than that of the CTGS-02 measurements with the constant term subtracted and, also, lower than those of all previously reported losses in other crystals in the langasite family. The material loss in this temperature range is found to be dominated by point defect relaxations, the presence of which is apparently not determined by the fundamental order or disorder of the crystal. On the other hand, the lower conductivity and associated loss of CTGS at the highest measured temperatures, relative to LGS, is largely attributable to the order of the crystal.

The minimization of the influence of point defects and conductivity-related relaxations at a given anticipated application temperature could be achieved by an appropriate choice of operating frequencies either by tailoring the fundamental mode frequency or by the use of higher harmonics.

It is still to be determined what type of point defects are responsible for relaxation peaks observed in CTGS, LGS, and LGT. Full impurity analyses will need to be performed on specimens to identify correlations of defect concentrations with Q^{-1} . Such research will need to consider that point-defect concentrations even at ppm levels can introduce significant contributions to the loss and conductivity, and the symmetry and associated anelastic contributions of defects can change when charge states of defects change.

ACKNOWLEDGMENTS

A research grant from the German Research Foundation (Nos. DFG: FR 1301/21-2 and SO 1085/2-2) supported this work. Furthermore, the authors from the Clausthal University of Technology acknowledge the support of the Energie-Forschungszentrum Nieder-sachsen, Goslar, Germany. Dr. S. Ganschow and co-workers from the Leibniz-Institut für Kristallzüchtung, Berlin, Germany, are thanked for providing the LGS resonator for the study. This manuscript is a contribution of the National Institute of Standards and Technology and is not subject to copyright in the United States.

DATA AVAILABILITY

The data that support the findings of this study are available from the corresponding author upon reasonable request.

REFERENCES

- ¹S. Zhang and F. Yu, "Piezoelectric materials for high temperature sensors," *J. Am. Ceram. Soc.* **94**, 3153–3170 (2011).
- ²H. Fritze, "High-temperature bulk acoustic wave sensors," *Meas. Sci. Technol.* **22**, 012002 (2011).
- ³H. Zu, H. Wu, and Q. Wang, "High-temperature piezoelectric crystals for acoustic wave sensor applications," *IEEE Trans. Ultrason. Ferroelectr. Freq. Control* **63**, 486–505 (2016).
- ⁴M. Rodahl, F. Höök, A. Krozer, P. Brzezinski, and B. Kasemo, "Quartz crystal microbalance setup for frequency and Q-factor measurements in gaseous and liquid environments," *Rev. Sci. Instrum.* **66**, 3924–3930 (1995).
- ⁵E. Benes, "Improved quartz microbalance technique," *J. Appl. Phys.* **56**, 608–626 (1984).
- ⁶D. Johannsmann, K. Mathauer, G. Wegner, and W. Knoll, "Viscoelastic properties of thin films probed with a quartz-crystal resonator," *Phys. Rev. B* **46**, 7808–7815 (1992).

- ⁷C. Behling, R. Lucklum, and P. Hauptmann, "Response of quartz-crystal resonators to gas and liquid analyte exposure," *Sens Actuators A* **68**, 388–398 (1998).
- ⁸A. Bund and G. Schwitzgebel, "Validation of the frequency shift of thickness-shear-mode resonators in liquids—Determination of the activation energy of viscosity," *Ber. Bunsenges. Phys. Chem.* **101**, 1960–1962 (1997).
- ⁹S. S. Narine and A. J. Slavin, "Use of the quartz crystal microbalance to measure the mass of submonolayer deposits: Measuring the stoichiometry of surface oxides," *J. Vac. Sci. Technol. A* **16**, 1857–1862 (1998).
- ¹⁰S. Schröder, H. Fritze, S. Bishop, D. Chen, and H. L. Tuller, "Thin-film nanothermogravimetry applied to praseodymium-cerium oxide films at high temperatures," *Appl. Phys. Lett.* **112**, 213502 (2018).
- ¹¹V. Segouin, B. Kaeswurm, K. G. Webber, and L. Daniel, "Temperature-dependent an hysteretic behavior of co-doped PZT," *J. Appl. Phys.* **124**, 104103 (2018).
- ¹²T.-L. Zhao, A. A. Bokov, J. Wu, H. Wang, C.-M. Wang, Y. Yu, C.-L. Wang, K. Zeng, Z.-G. Ye, and S. Dong, "Giant, piezoelectricity of ternary perovskite ceramics at high temperatures," *Adv. Funct. Mater.* **29**, 1807920 (2019).
- ¹³D. Damjanovic, "Materials for high-temperature piezoelectric transducers," *Curr. Opin. Solid State Mater. Sci.* **3**, 469–473 (1998).
- ¹⁴T. Uno, H. Tashiro, and S. Noge, "Temperature characteristics of β -phase quartz resonators and their application to accurate temperature sensors in high-temperature region," *Electron. Commun. Jpn.* **95**, 9–18 (2012).
- ¹⁵D. P. Birnie III, "Analysis of diffusion in lithium niobate," *J. Mater. Sci.* **28**, 302–315 (1993).
- ¹⁶E. J. Samuelsen and A. P. Grande, "The ferroelectric phase transition in LiTaO_3 studied by neutron scattering," *Z. Phys. B Condens. Matter* **24**, 207–210 (1976).
- ¹⁷A. Weidenfelder, J. Shi, P. Fielitz, G. Borchardt, K. D. Becker, and H. Fritze, "Electrical and electromechanical properties of stoichiometric lithium niobate at high-temperatures," *Solid State Ionics* **225**, 26–29 (2012).
- ¹⁸D. A. Parks, S. Zhang, and B. R. Tittmann, "High-temperature (>500 °C) ultrasonic transducers: An experimental comparison among three candidate piezoelectric materials," *IEEE Trans. Ultrason. Ferroelectr. Freq. Control* **60**, 1010–1015 (2013).
- ¹⁹I. Kogut, C. Hartmann, I. Gamov, Y. Suhak, M. Schulz, S. Schröder, J. Wollweber, A. Dittmar, K. Irmischer, T. Straubinger, M. Bickermann, and H. Fritze, "Electromechanical losses in carbon- and oxygen-containing bulk AlN single crystals," *Solid State Ionics* **343**, 115072 (2019).
- ²⁰C. Hartmann, A. Dittmar, J. Wollweber, and M. Bickermann, "Bulk AlN growth by physical vapour transport," *Semicond. Sci. Technol.* **29**, 084002 (2014).
- ²¹J. Haines, O. Cambon, N. Prudhomme, G. Fraysse, D. Keen, L. Chapon, and M. Tucker, "High-temperature, structural disorder, phase transitions, and piezoelectric properties of GaPO_4 ," *Phys. Rev. B* **73**, 014103 (2006).
- ²²E. Philippot, A. Ibanez, A. Goiffon, M. Cochez, A. Zarka, B. Capelle, J. Schwartzel, and J. Detaint, "A quartz-like material: Gallium phosphate (GaPO_4); crystal growth and characterization," *J. Cryst. Growth* **130**, 195–208 (1993).
- ²³X. Jiang, K. Kim, S. Zhang, J. Johnson, and G. Salazar, "High-temperature piezoelectric sensing," *Sensors* **14**, 144–169 (2014).
- ²⁴S. Zhang, E. Frantz, R. Xia, W. Everson, J. Randi, D. W. Snyder, and T. R. Shrout, "Gadolinium calcium oxyborate piezoelectric single crystals for ultrahigh temperature (>1000 °C) applications," *J. Appl. Phys.* **104**, 084103 (2008).
- ²⁵H. Ohsato, T. Iwataki, and H. Morikoshi, "Crystal structure and piezoelectric properties of four component langasite $\text{A}_3\text{BGa}_3\text{Si}_2\text{O}_{14}$ (A = Ca or Sr, B = Ta or Nb)," *Trans. Electr. Electron. Mater.* **13**, 171–176 (2012).
- ²⁶H. Fritze, H. L. Tuller, G. Borchardt, and T. Fukuda, "High-temperature properties of langasite," *MRS Proc.* **604**, 65–70 (1999).
- ²⁷K. Shimamura, H. Takeda, T. Kohno, and T. Fukuda, "Growth and characterization of lanthanum gallium silicate $\text{La}_3\text{Ga}_5\text{SiO}_{14}$ single crystals for piezoelectric applications," *J. Cryst. Growth* **163**, 388–392 (1996).
- ²⁸B. V. Mill and Y. V. Pisarevsky, "Langasite-type materials: From discovery to present state," in *Proceedings of the IEEE/EIA International Frequency Control Symposium* (IEEE, 2000), pp. 133–144.
- ²⁹J. Stade, L. Bohaty, M. Hengst, and R. B. Heimann, "Electro-optic, piezoelectric and dielectric properties of langasite ($\text{La}_3\text{Ga}_5\text{SiO}_{14}$), langanite ($\text{La}_3\text{Ga}_{5.5}\text{Nb}_{0.5}\text{O}_{14}$) and langatate ($\text{La}_3\text{Ga}_{5.5}\text{Ta}_{0.5}\text{O}_{14}$)," *Cryst. Res. Technol.* **37**, 1113–1120 (2002).
- ³⁰S. Zhang, Y. Zheng, H. Kong, J. Xin, E. Frantz, and T. R. Shrout, "Characterization of high temperature piezoelectric crystals with an ordered langasite structure," *J. Appl. Phys.* **105**, 114107 (2009).
- ³¹Y. Suhak, M. Schulz, H. Wulfmeier, W. L. Johnson, A. Sotnikov, H. Schmidt, S. Ganschow, D. Klimm, and H. Fritze, "Langasite-type resonant sensors for harsh environments," *MRS Adv.* **1**, 1513–1518 (2016).
- ³²H. Fritze and H. L. Tuller, "High-temperature balance," U.S. patent No. 6,370,955 (2002).
- ³³J. Schreuer, C. Thybaut, M. Prestat, J. Stade, and E. Haussühl, "Towards an understanding of the anomalous electromechanical behaviour of langasite and related compounds at high temperatures," in *IEEE International Ultrasonics Symposium* (IEEE, 2003), pp. 196–199.
- ³⁴W. L. Johnson, S. Kim, S. Uda, and C. F. Rivenbark, "Acoustic damping in resonators of langasite and langatate at elevated temperatures," in *IEEE Sensors Symposium* (IEEE, 2011), pp. 1636–1639.
- ³⁵H. Fritze, M. Schulz, H. Seh, H. L. Tuller, S. Ganschow, and K. Jacobs, "High-temperature electromechanical properties of strontium-doped langasite," *Solid State Ionics* **177**, 3171–3174 (2006).
- ³⁶H. Fritze, "High temperature piezoelectric crystals and devices," *J. Electroceram.* **26**, 122–161 (2011).
- ³⁷W. L. Johnson, S. A. Kim, S. Uda, and C. F. Rivenbark, "Contributions to anelasticity in langasite and langatate," *J. Appl. Phys.* **110**, 123528 (2011).
- ³⁸C. Hirschele and J. Schreuer, "High-temperature ultrasound attenuation in langasite and langatate," *IEEE Trans. Ultrason. Ferroelectr. Freq. Control* **65**, 1250–1257 (2018).
- ³⁹Y. Suhak, M. Schulz, W. L. Johnson, A. Sotnikov, H. Schmidt, and H. Fritze, "Electromechanical properties and charge transport of $\text{Ca}_3\text{TaGa}_3\text{Si}_2\text{O}_{14}$ (CTGS) single crystals at elevated temperatures," *Solid State Ionics* **317**, 221–228 (2018).
- ⁴⁰W. L. Johnson, M. Schulz, and H. Fritze, "High-temperature electroacoustic characterization of Y-cut and singly-rotated $\text{Ca}_3\text{TaGa}_3\text{Si}_2\text{O}_{14}$ resonators," *IEEE Trans. Ultrason. Ferroelectr. Freq. Control* **61**, 1433–1441 (2014).
- ⁴¹W. L. Johnson, M. Schulz, and H. Fritze, "Acoustic and electrical properties of $\text{Ca}_3\text{TaGa}_3\text{Si}_2\text{O}_{14}$ piezoelectric resonators at elevated temperatures," in *IEEE Sensors Symposium* (IEEE, 2013), pp. 1–4.
- ⁴²Y. Suhak, W. L. Johnson, A. Sotnikov, H. Schmidt, and H. Fritze, "Transport and electromechanical properties of $\text{Ca}_3\text{TaGa}_3\text{Si}_2\text{O}_{14}$ piezoelectric crystals at extreme temperatures," *MRS Adv.* **4**, 515–521 (2019).
- ⁴³D. Richter, S. Sakharov, E. Forsen, E. Mayer, L. Reindl, and H. Fritze, "Thin film electrodes for high temperature surface acoustic wave devices," *Proc. Eng.* **25**, 168–171 (2011).
- ⁴⁴T. Ikeda, *Fundamentals of Piezoelectricity* (Oxford University Press, Oxford, 1990).
- ⁴⁵W. Johnson, "Ultrasonic resonance of metallic spheres at elevated temperatures," *J. Phys. IV* **6**(C8), 849 (1996).
- ⁴⁶W. P. Mason, *Physical Acoustics, Principles and Methods* (Academic Press, New York, 1965), Vol. 3B.
- ⁴⁷R. Tabrizian, M. Rais-Zadeh, and F. Ayazi, "Effect of phonon interactions on limiting the fQ product of micromechanical resonators," in *IEEE Transducers* (IEEE, 2009), pp. 2131–2134.
- ⁴⁸L. Landau and G. Rumer, *The Theory of Phase Transitions* (Pergamon Press, Oxford, 1936).
- ⁴⁹A. Akhiezer, "On the absorption of sound in solids," *J. Phys. (Moscow)* **1**, 277–287 (1939).
- ⁵⁰J. Rodriguez, S. A. Chandorkar, C. A. Watson, G. M. Glaze, C. H. Ahn, E. J. Ng, Y. Yang, and T. W. Kenny, "Direct detection of akhiezer damping in a silicon MEMS resonator," *Sci. Rep.* **9**, 2244 (2019).
- ⁵¹A. S. Nowick and B. S. Berry, *Anelastic Relaxation in Crystalline Solids* (Academic Press, New York, 1972).

- ⁵²A. R. Hutson and D. L. White, "Elastic wave propagation in piezoelectric semiconductors," *J. Appl. Phys.* **33**, 40–47 (1962).
- ⁵³Y. Suhak, M. Schulz, A. Sotnikov, H. Schmidt, S. Ganschow, S. Sakharov, and H. Fritze, "Dielectric, piezoelectric and elastic constants of $\text{Ca}_3\text{TaGa}_3\text{Si}_2\text{O}_{14}$ single crystals at elevated temperatures," *Integr. Ferroelectr.* **537**, 255–263 (2018).
- ⁵⁴H. Seh and H. L. Tuller, "Defects and transport in langasite II: Donor-doped ($\text{La}_3\text{Ga}_{4.75}\text{Nb}_{0.25}\text{SiO}_{14}$)," *J. Electroceram.* **15**, 193–202 (2005).
- ⁵⁵A. Ballato, "Electronic activity dip measurement," *IEEE Trans. Instrum. Meas.* **27**, 59–65 (1978).
- ⁵⁶R. C. Smythe, R. C. Helmbold, G. E. Hague, and K. A. Snow, "Langasite, langanite, and langatate bulk-wave Y-cut resonators," *IEEE Trans. Ultrason. Ferroelectr. Freq. Control* **47**, 355–360 (2000).
- ⁵⁷H. Seh, H. Fritze, and H. L. Tuller, "Defect chemistry of langasite III: Predictions of electrical and gravimetric properties and application to operation of high temperature crystal microbalance," *J. Electroceram.* **18**, 139–147 (2007).
- ⁵⁸M. Wehnacht, A. Sotnikov, H. Schmidt, B. Wall, and R. Grünwald, "Langasite: High temperature properties and SAW simulations," in *IEEE International Ultrasonics Symposium* (IEEE, 2012), pp. 1549–1552.
- ⁵⁹P. K. Grewal and M. J. Lea, "Ultrasonic attenuation in pure and doped $\text{Bi}_{12}\text{GeO}_{20}$," *J. Phys. C: Solid State Phys.* **16**, 247–257 (1983).
- ⁶⁰A. Li, Y. N. Wang, X. N. Ying, Q. M. Zhang, and W. M. Chen, "Effect of zinc substitution on internal friction in YBCO superconductors," *Supercond. Sci. Technol.* **12**, 645–648 (1999).
- ⁶¹X. Wang and J. Z. Wu, "Effect of temperature and magnetic field on the thickness dependence of the critical current density of $\text{YBa}_2\text{Cu}_3\text{O}_{7-x}$ films," *Phys. Rev. B* **76**, 184508 (2007).
- ⁶²M. Weller, "Anelastic relaxation of point defects in cubic crystals," *J. Phys. IV* **6**(C8), 63–72 (1996).
- ⁶³S. Jen, B. C. C. Teng, M. M. C. Chou, B. H. T. Chai, T. T. Lee, and J. Gwo, "Experimental investigation of the BAW device potentials of singly rotated Y-cut ordered langasite-structure crystals," in *Proceedings of the IEEE International Frequency Control Symposium* (IEEE, 2002), pp. 307–310.
- ⁶⁴F. Yu, X. Zhao, L. Pan, F. Li, D. Yuan, and S. Zhang, "Investigation of zero temperature compensated cuts in langasite-type piezocrystals for high temperature applications," *J. Phys. D: Appl. Phys.* **43**, 165402 (2010).